Ageing behaviour of composite rocket propellant formulations investigated by DMA, SGA and GPC

Manfred A. Bohn*, Sara Cerri*,**

* Fraunhofer ICT, 76318 Pfinztal-Berghausen, Postfach 1240, Germany
** Dipartimento di Energia, Politecnico di Milano, Milano, Italy

Abstract

Solid rocket propellants (SRP) based on HTPB / AP / Al (binder hydroxyl terminated polybutadiene / ammonium perchlorate / aluminium powder) are at time the choice to achieve high performance with high specific impulses. Such propellants change their properties with time. Ageing mechanisms are: after-curing, chain rupture by mechanical overload during temperature cycling, oxidative hardening together with loss in strain capability, oxidative chain scissioning, dewetting between particulate fillers (especially AP) and binder matrix. In this work DMA (Dynamic Mechanical Analysis) in torsion mode and Sol-Gel-Analysis (SGA) have been employed together with SEM (Scanning Electron Microscopy) and GPC (Gel Permeation Chromatography) to elucidate the ageing behaviour of four HTPB-based SRP, whereby the particle size of aluminium powder was changed also. The accelerated ageing range was between 60°C and 90°C with ageing times adjusted to a thermal equivalent load of 15 to 20 years at 25°C. The investigations with DMA revealed distinct changes in the shape of the loss factor curve. The loss factor gives the part of applied deformation energy, which is consumed by the sample. The other part is transported through the sample to the response detector. Detailed analysis of the shape of the loss factor showed that three parts of molecular rearrangement types can be identified during the total transition of the material from energy-elastic to the entropy-elastic state. The results of SGA showed a complex change in soluble or extractable polymeric binder part. Both cross-linking and to some part also chain scissioning occur, which could be recognized by the changes of the molar mass distribution functions of the extractable binder part.

Keywords
HTPB propellants, ageing, DMA, Sol-Gel analysis, gel permeation chromatography, loss factor evaluation, molecular mobility changes

1   Introduction

Rocket propellant formulations based on AP/Al (ammonium perchlorate/aluminium) and HTPB (hydroxyl terminated polybutadiene) are at time the state-of-the-art in the current western solid rocket motors (SRMs). They enable to achieve high performances with high specific gravimetric (I_{sp}) and volumetric (I_{spv}) impulses. The use of the HTPB pre-polymer offers a good combination of mechanical and ballistic properties. The oxidiser AP is chosen because it shows acceptable sensitivity, good thermal stability, high density and high oxygen balance (O.B.). However, AP-based propellants produce hydrogen chloride as combustion product causing on one hand signature and on the other hand severe corrosion and environmental risks as fostering ozone depletion. The use of aluminium powders has the purpose to increase the ballistic properties of the propellant formulations. The combustion of the aluminium with the oxygen coming from the decomposition of the oxidiser gives a highly exothermic reaction, which leads to an increase in the flame temperature (T_c) and of the I_{sp} despite of an increase of the average molecular mass of the combustion products. In principle, the use of nanoAl can give remarkable

improvements in the ballistic performances of the standard HTPB/AP formulations. Many studies have been carried out mainly in the ballistic field. Very few studies have investigated the effect of these high specific surface particles on the mechanical properties and on the ageing behaviour of the final system. In this work DMA (Dynamic Mechanical Analysis) in torsion mode and Sol-Gel-Analysis (SGA) were employed together with SEM and GPC (Gel Permeation Chromatography) to elucidate the ageing behaviour of four HTPB-based SRP, whereby the particle size of the aluminium powder and its content were changed. The accelerated ageing range was between 60°C and 90°C with ageing times adjusted to a thermal equivalent load of 15 years at 25°C, in part also 20 years at 25°C.

2 Experimental

2.1 Formulations

Four HTPB/AP/Al-based formulations were investigated, which have been manufactured at Fraunhofer ICT. They were divided into two groups in order to study the influence of the Al content and average particle size: the formulations named AV03 and AV05 contain 6 mass-% of Al, while the formulations called AV04 and AV06 have 12 mass-% of Al particles. Details of the formulations are shown in Table 1. Propellants AV03 and AV04 have micrometric aluminium (Alcan, Grade X-81, 8 µm, Lot. SI 23289, Eckart, Austria). Propellant AV05 has only nanometric aluminium inside (ALEX, 100-200 nm, USA), AV06 has a 6 mass-% of nanoAl and a 6 mass-% of microAl (8 µm). All the formulations were prepared in a vertical kneader (Drais T FHG, Germany) having a volume of 5 l and cured in an electrical oven cabinet (from company Memmert, Germany) for two days at 60°C. In order to have not too high end of mix viscosity (EOMV) and problems of propellant castability [1,2,3], the fraction of nanoAl inserted into the material was limited to 6 mass-%.

Table 1: Compositions of the studied formulations. The equivalent ratio R_{eq} (NCO/OH) contains also the Tepanol part: OH = HTPB-OH + Tepanol-OH.

Component / property		AV03	AV04	AV05	AV06
AP 5.4 µm	[m.-%]	6	-	6	-
AP 45 µm	[m.-%]	24	24	24	24
AP 200 µm	[m.-%]	48	48	48	48
micro-Al (18 µm)	[m.-%]	6	12	-	6
nano-Al (100-200 nm)	[m.-%]	-	-	6	6
HTPB R45M[TM]	[m.-%]	10.72	10.72	10.72	10.72
DOA	[m.-%]	4	4	4	4
HX-878 (Tepanol[TM])	[m.-%]	0.19	0.19	0.19	0.19
Irganox[TM] 565	[m.-%]	0.2	0.2	0.2	0.2
IPDI	[m.-%]	0.89	0.89	0.89	0.89
TPB	[m.-%]	0.02	0.02	0.02	0.02
Solid load	[m.-%]	84	84	84	84
Plasticizer part of binder	[m.-%]	25	25	25	25
Oxygen balance O.B.	[%]	-26.51	-33.89	-26.51	-33.89
Theoretical density ρ_{th}	[g·cm^{-3}]	1.693	1.718	1.693	1.718
R_{eq} (NCO/OH)	[-]	0.87	0.87	0.87	0.87

2.2 Sample preparation and ageing conditions

A thermal accelerated ageing programme was carried out in PID temperature-controlled (± 0.5°C) ageing ovens (design based on former company Julius Peters, Berlin). The aim of the

study was the evaluation of the accelerated ageing of the surface-layer of solid rocket propellants (no 'in core' analysis), so specimens were aged at 60, 70, 80, 85 and 90°C in air (RH<10%) to simulate 15 to 20 years of natural ageing. To establish the ageing plan the principle of Thermal Equivalent Load (TEL) was used together with the generalized van't Hoff rule [4].

Table 2: Applied accelerated ageing conditions (temperatures and times) simulating an in-service time of up to 20 years at 25°C. Ageing conditions determined using the TEL principle and thermal load simulation based on the generalised van't Hoff rule [4] with a scaling factor of 2.5 per 10°C temperature change. The given ageing times are rounded up.

Natural or in-service ageing			
In service temperature T_E [°C]	In-service time t_E [year]		
25	5	10	15	20
Accelerated ageing conditions based on TEL principle using van't Hoff with F = 2.5			
Ageing temperature T_T [°C]	Ageing time t_T [day]		
90	5	10	15	20
85	7.5	15	22.5	30
80	12	24	36	48
70	30	60	90	120
60	75	150	225	300

The specimens for the DMA measurements and for the Sol-Gel analyses were aged in a so called 'ready-to-test' geometry, means they have had the final dimensions. Small rectangular bars with dimensions of 10mm wide, 4 to 5mm thick and 50mm long, were considered for the DMA measurements, while for the SGA small pieces of material (roughly 1-2mm x 2mm x 2mm) were cut. The samples were stored in glass tubes having also ground glass stoppers. The stoppers were not fixed with a clamp and not sealed by grease. Therefore a little bit of air and of humidity could go inside and volatiles from the propellants could flow outside. Twice a week the stoppers have been removed and fresh air could flow inside. Because the specimens for the SG measurements were so small, the glass tubes were shaken in order to give fresh air to all the specimens.

2.2.1   DMA measurements

All the dynamic mechanical measurements were carried out in torsion mode using a DMA instrument of type ARES™ (Advanced Rheometric Expansion System) manufactured by Rheometric Scientific (now belonging to Waters, Inc, BU TA Instruments). A liquid-nitrogen cooling accessory was used for the low and high temperature operations. The temperature range was -100°C to 70°C, with the heating rate of 1°C·min⁻¹ and soak time of 28 s. The specimens were tested at four deformation frequency values (0.1, 1.0, 10.0, 56.0Hz) using a strain control with maximum strain of 0.0012, in order to stay in the linear range domain and not to induce Payne effects. The measurement reproducibility of these measurements is very high so only one sample per each test condition was used. In the case of anomalous behaviour a second measurement was performed.

2.2.2   Sol-Gel measurements

The oxidative ageing of the composite propellants was investigated with the Sol-Gel Analysis (SGA). The soluble or extractable content is a useful parameter to characterise the extent of cross-linking or chain scissioning within a cross-linked polymer. The greater the fraction of not cross-linked polymer chains, the higher the soluble fraction. If the cross-linking predominates, an insoluble macroscopic gel will be formed. The sol content of the binder of the propellant

(S_{prop}) is the weight fraction of the propellant, which is obtained by extraction with solvent, as described in STANAG 4581. It contains all extractable parts, also plasticisers and antioxidants.

$$S_{prop} = \frac{(W_2 - W_3)}{(W_2 - W_1)} = \frac{E_{total}}{A} . \tag{1}$$

S_{prop} total soluble (extractable) part in the propellant sample [-];
E_{total} total amount of extract gained by the method [g];
W_1 mass of the dry glass extraction tube at start [g];
W_2 mass of the extraction tube + mass of the sample before the extraction [g];
W_3 mass of the extraction tube + mass of the sample after the extraction (after drying) [g];
A weighed-in amount of propellant for the extraction [g].

A known mass of propellant was added to a weighed dry glass extraction tube having a glass filter (porosity 3). The extractions were carried out in triplicate and an average value was obtained. The extraction tubes were dried by heating in a vacuum oven for 3 hours at 50°C. They were cooled for one hour in a desiccator containing dry silica gel and then weighed accurately (W_1 [g]). 3.0±0.1 g of small specimens (1-2mm x 2mm x 2mm) were added for each extraction tube and then the tubes were reweighed (W_2 [g]). The extraction was carried out in three Soxhlet extraction units (refluxing with solvent) for 16 hours with 150ml of dichloromethane CH_2Cl_2 each (overnight procedure). Then the extraction tubes were removed, the excess solvent was allowed to evaporate under a fume cupboard for some hours, but at least two hours. The extraction tubes were placed in the vacuum oven at 50°C for 16 hours (overnight procedure). After that they were transferred for one hour in a desiccator containing dry silica gel and reweighed (W_3 [g]). The use of so small specimens reduce the problems linked with the DLO (diffusion limited oxidation) effects. The solutions obtained by the extraction contained the total extractable soluble fraction and were retained for the GPC measurements.

2.2.3 GPC measurements

Gel permeation chromatography (GPC) measurements were applied to get information about the molecular mass distributions of the polymeric binder extracts and the content of the other extractable ingredients (plasticiser and antioxidant). GPC, also named Size Exclusion Chromatography (SEC), separates dissolved polymer molecules according to their hydrodynamic size (volume) in the used solvent by passing a porous gel enclosed in high pressure columns. The largest molecules are eluated first and the smallest are detected at last. With organic polymers dissolvable in organic solvents as THF (tetrahydrofurane) divinylbenzene cross-linked polystyrene gel is mostly used as separating phase. By suitable calibration the GPC method can be used also to quantify the content of monomolecular ingredients in the extracts as the plasticiser DOA and the antioxidant Irganox 565. The solvent of the extraction solution (solvent+soluble fraction) was removed through a rotary evaporator. At the beginning the procedure was done by removing most of the CH_2Cl_2 with a membrane pump. Then the residual material was transferred in small glasses having a volume of 10ml and the rotary evaporation was done with an oil pump, in order to remove completely the solvent.

GPC was performed with instruments from Agilent series 1100 including a refractive index (RI) detector. A solvent online degasser was used. The column set was assembled with four single porosity columns in series of type PSS SDV from company PSS Polymer Standards Service GmbH, Mainz, Germany. The pore sizes have been 50, 100, 1000 and 100000 Å, the outer column diameter was 8.0 mm and the length 300 mm. As eluent as well as sample solvent THF was used at a flow rate of 1 ml·min^{-1}. Calibration of the column set was achieved with 19 narrowly distributed polystyrene standards well positioned along the calibration curve. Sample injection volume was 100µl and sample concentration in THF was in average around 3mg·ml^{-1}. For further parameters and conditions see Appendix: GPC measurement conditions.

2.2.4   SEM analyses

Scanning electron microscopy (SEM) analyses were performed using the scanning electron microscope Supra 55 VP manufactured by company ZEISS, Germany. The slices of propellant cut for the Sol-Gel-Analysis were analysed in order to put in evidence possible dewetting phenomena during the swelling of the material.

3   Results

3.1   DMA measurements

The propellant specimens were analysed in torsion mode. This mode enables to determine the binder characteristics without distortions due to the particle-particle contact as it can happen in tensile-compression mode or in bending mode especially for the highly filled composite propellants. No slip in the sample mounting can be evidenced and no needs to glue the sample to the specimen holders are necessary. The only disadvantage can derive from a not equal straining along the sample width if large strain amplitudes are applied. In order to prevent this, the maximum used strain was limited to 0.0012.
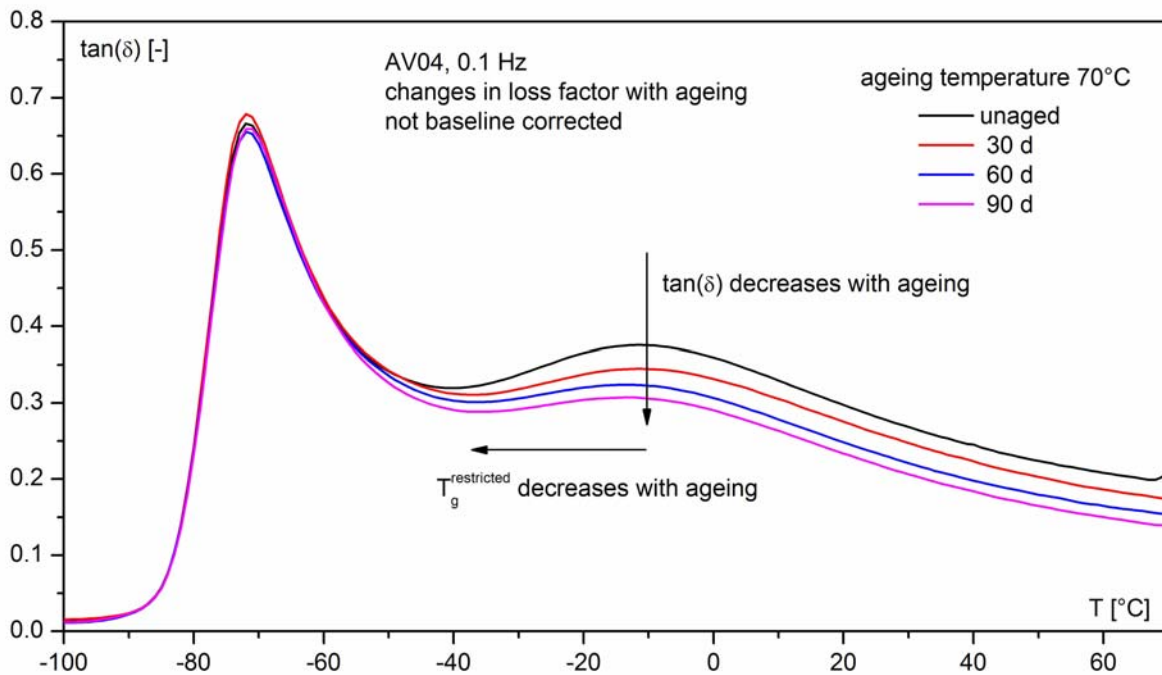
Figure 1: Loss factor vs. temperature for AV04 formulation as function of ageing at 70°C.

Fig. 1 shows the trend of the loss factor $\tan(\delta)=G''/G'$ with ageing, where G' is the storage shear modulus and G" is the loss shear modulus. Based on a weakly cross-linked polymeric matrix, solid rocket propellants show very large changes in mechanical properties with changing temperature. For every ageing time the presence of two maxima in the loss factor can be seen. The first maximum is deformation frequency dependent and located between -80°C and -60°C (depending on the applied deformation frequency); the second maximum is deformation frequency dependent too but is broader than the first one and appears at higher temperatures. Weekly cross-linked elastomers change from a glass-like to rubber-like behaviour as the temperature is increased. In the glassy state, at low temperature, the behaviour is related to the changes in the stored elastic energy by small displacements of the molecules from their equilibrium positions. In the rubbery state at high temperatures, the molecular chains have much more flexibility and can adopt a large number of conformations, which lead to a maximum of

entropy. Scanning the temperature from one state region to the other the material passes an in-between region, where the transitions occur as molecular rearrangements. Generally, this phenomenon is named glass transition and the associated temperature range glass transition region.
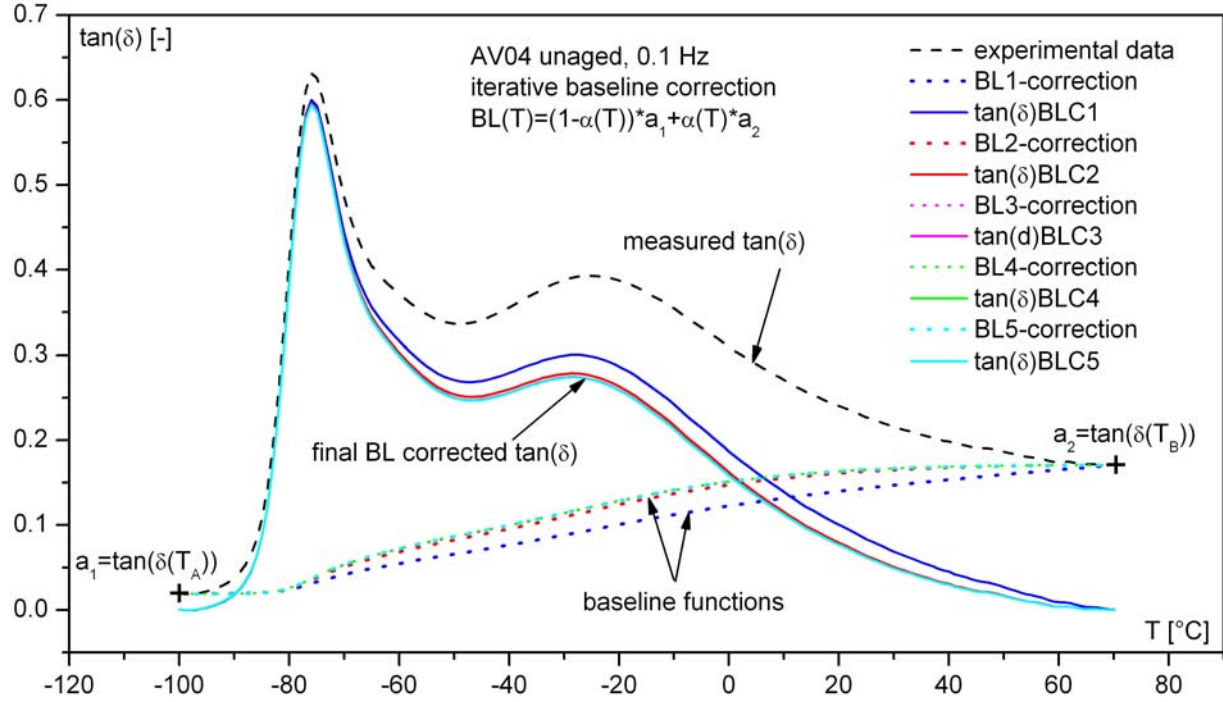

Figure 2: Illustration of the baseline correction (BLC) of the loss factor curve of the unaged propellant formulation AV04 as example.

The energy used during the DMA measurements is in part transmitted loss free from the donor to the acceptor of the specimen holder during the measurement and in part used up by the propellant specimen. This second phenomenon has two contributions: a purely dissipative one in which the energy is transformed to heat by frictional effects, and a contribution used for the molecular rearrangements. The rearrangement energy is taken up to separate the molecular chains. Outside the glass transition regions only dissipative consumptions occur, which are usually small, particularly in the energy-elastic state. Considering unfilled elastomers they are small also in the entropy-elastic state. Indeed, with filled elastomers these dissipative effects become significant. In order to extract the information concerning the molecular mobility interpretation of the loss factor these dissipative effects must be separated. A visual sign for the dissipative part is the baseline offset between the start and the end point of the distribution (Fig. 2). The separation of the dissipative part can be done 'geometrically' by applying a suitable iterative baseline correction shown in Eq.(2), using a transient function $\alpha(T)$, Eq.(3), a cumulative partition variable, to adjust the baseline weights along the loss factor curve.

$$BL(T) = \left(1 - \alpha(T)\right) \cdot \tan(\delta(T_A)) + \alpha(T) \cdot \tan(\delta(T_B)). \tag{2}$$

$$\alpha(T) = \frac{\int\limits_{T_a}^{T} \tan(\delta)\,dT}{\int\limits_{T_a}^{T_b} \tan(\delta)\,dT}. \tag{3}$$

BL(T)	base line correction function between T_A and T_B
$\alpha(T)$	cumulative partition variable of $\tan\delta(T)$
T_A	lower baseline setting temperature [°C]
T_B	upper baseline setting temperature [°C]

T	actual measurement temperature between T_A and T_B [°C]
$\tan\delta(T_A)$	value of $\tan\delta(T)$ at temperature T_A
$\tan\delta(T_B)$	value of $\tan\delta(T)$ at temperature T_B

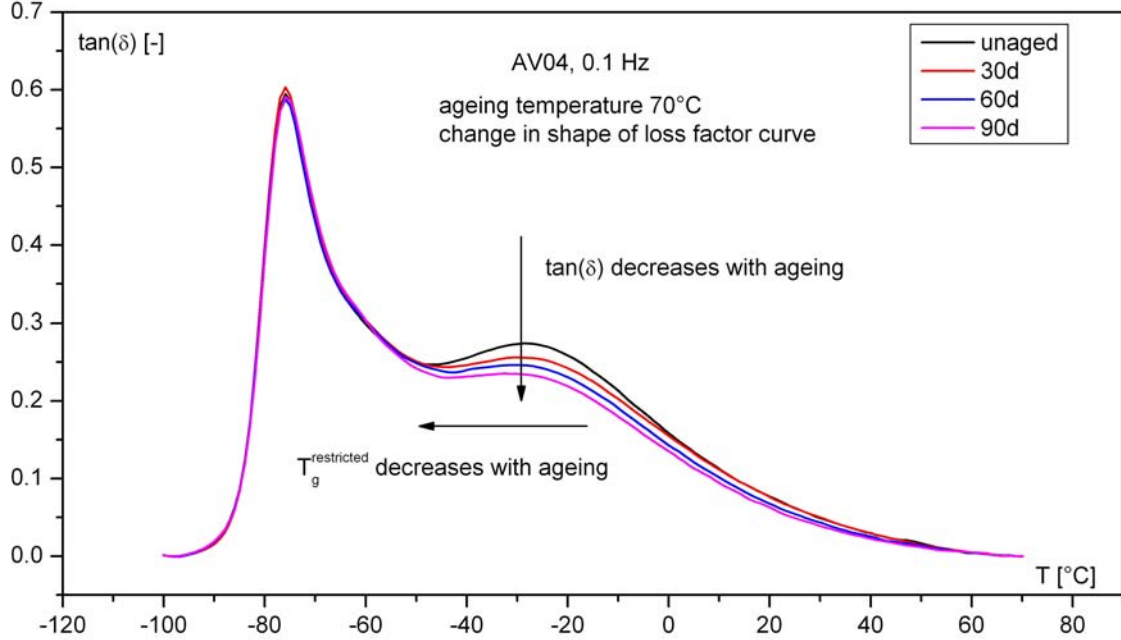A more detailed discussion can be found in paper [21].

Figure 3: Baseline corrected loss factor curve vs. temperature at different ageing times for the aged AV04 formulation (ageing temperature=70°C).

Fig. 3 shows the corrected loss factor curves after the baseline correction (BLC) step. Regarding the first peak, the behaviour of the aged and unaged propellant is similar. The values of the temperatures corresponding to these maxima agree with those obtained with DSC measurements and are only slightly influenced by ageing [5]. However, remarkable changes are associated with the area of the second peak.

After the baseline correction a suitable fit function must be chosen in order to evaluate correctly the area under the second peak. Some fitting functions were analysed in another paper [6]. The function must describe the experimental data and extract from it the changes in the molecular structure. If the values of the molecular interaction energies and the molecular docking regions are randomly distributed in the isotropic material, a Gauss distribution (Eq. 4) should describe the processes. But, as clearly visible in Fig. 2 and 3, the shapes of the loss factor curves are not symmetrical as a Gauss distribution, meaning that some dissipative parts still remain in the experimental data. These dissipative effects can be described with relaxation curves, which mostly can be represented with exponentially decreasing functions (Eq. 5). These combined processes are described by an exponentially modified Gauss distribution function (EMG), shown in Eq. 6. There a sum of EMGs is given, because the whole loss factor curve is composed of several transition process types. The use of only two EMGs is not sufficient to describe well the valley region between the two peaks [6], therefore a value of N equal 3 was used.

$$f_G(T) = \frac{A}{w \cdot \sqrt{2}} \cdot \exp\left[-0.5 \cdot \left(\frac{T - Tc}{w}\right)^2\right] \tag{4}$$

$$f_E(T) = \exp\left(-\frac{T}{\tau}\right) \tag{5}$$

$$\tan(\delta)_{BLC} = td_0 + \sum_{i=1}^{N} \frac{A_i}{\tau_i} \cdot \frac{1}{2} \cdot \exp\left[0.5 \cdot \left(\frac{w_i}{\tau_i}\right)^2 - \frac{T - Tc_i}{\tau_i} \right] \left\{ 1 - \mathrm{erf}\left[-\frac{1}{\sqrt{2}} \cdot \left(\frac{T - Tc_i}{w_i} - \frac{w_i}{\tau_i}\right) \right] \right\} \quad (6)$$

T = measurement temperature [°C];

$\tan(\delta)_{BLC}$ = value of the loss factor after the baseline correction (BLC) as function of T [-];

A_i = area of the EMG peak, also equivalent to the area of the Gauss peak alone [°C];

w_i = half peak width at half height of only Gaussian part [°C];

Tc_i = temperature at peak maxima in the Gaussian part of EMG (not the peak maxima of EMG) [°C];

τ_i = relaxation parameter in exponential part of EMG [°C];

td_0 = residual offset in $\tan(\delta)$ data [-], for the evaluations made here the value was fixed equal to 0;

N = number of EMG fit functions;

erf = error function.

Fig. 4 shows an example of EMG peaks together with their Gauss parts. In order to simplify the figure, the considerations, the BLC experimental data of the loss factor were described only with two EMG functions. As can be seen for both the EMGs, the maximum of their peaks lie on the corresponding Gaussian curves. Depending on the relative weight of the dissipative part, the EMG functions are moving from the maximum of the Gauss curves to the base, meaning totally dissipative behaviours. In Fig. 5 the description of the loss factor of the unaged AV04 propellant formulation with three EMGs is presented. This data treatment was done for three unaged and aged propellant formulations (AV03, AV04, AV05) in order to follow the molecular changes with ageing. The aged values of the propellant formulations containing a mixture of nanometric and micrometric Al are not shown here due to some experimental problems encountered during the measurement campaign.
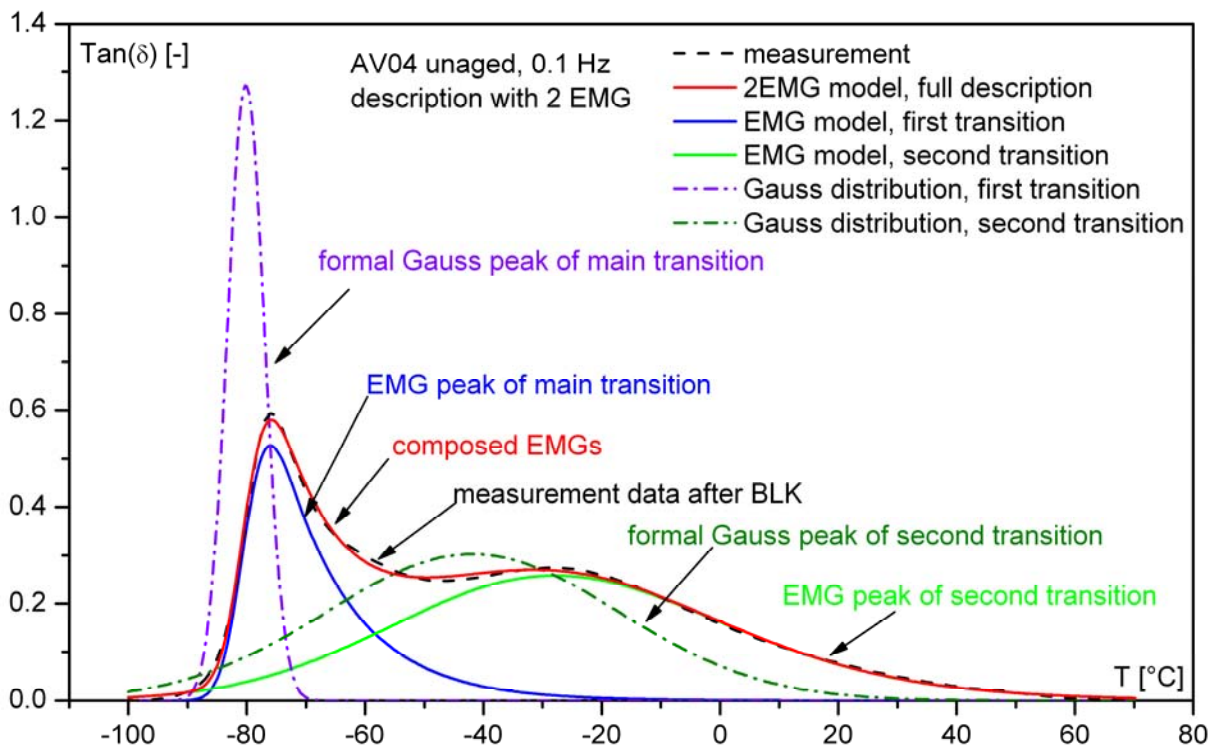

Figure 4: Detailed representation of the formal Gauss peak and EMG peak of the main and second transition considering only two EMG functions.
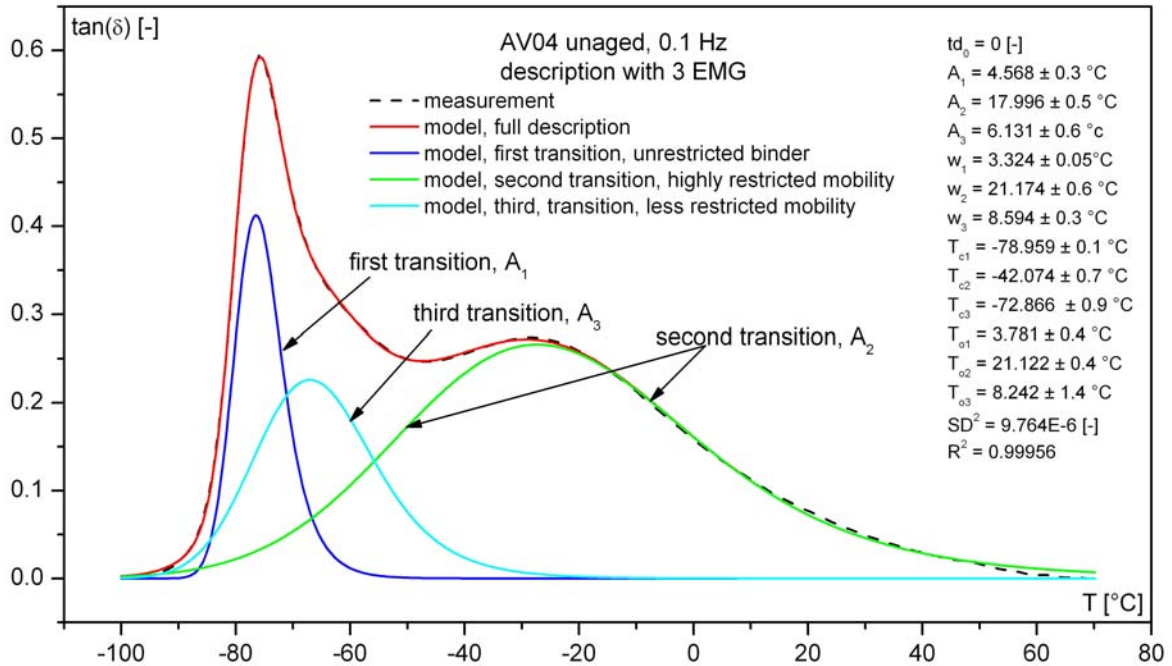
Figure 5: Description of the loss factor of the unaged AV04 propellant formulation with three EMG functions.
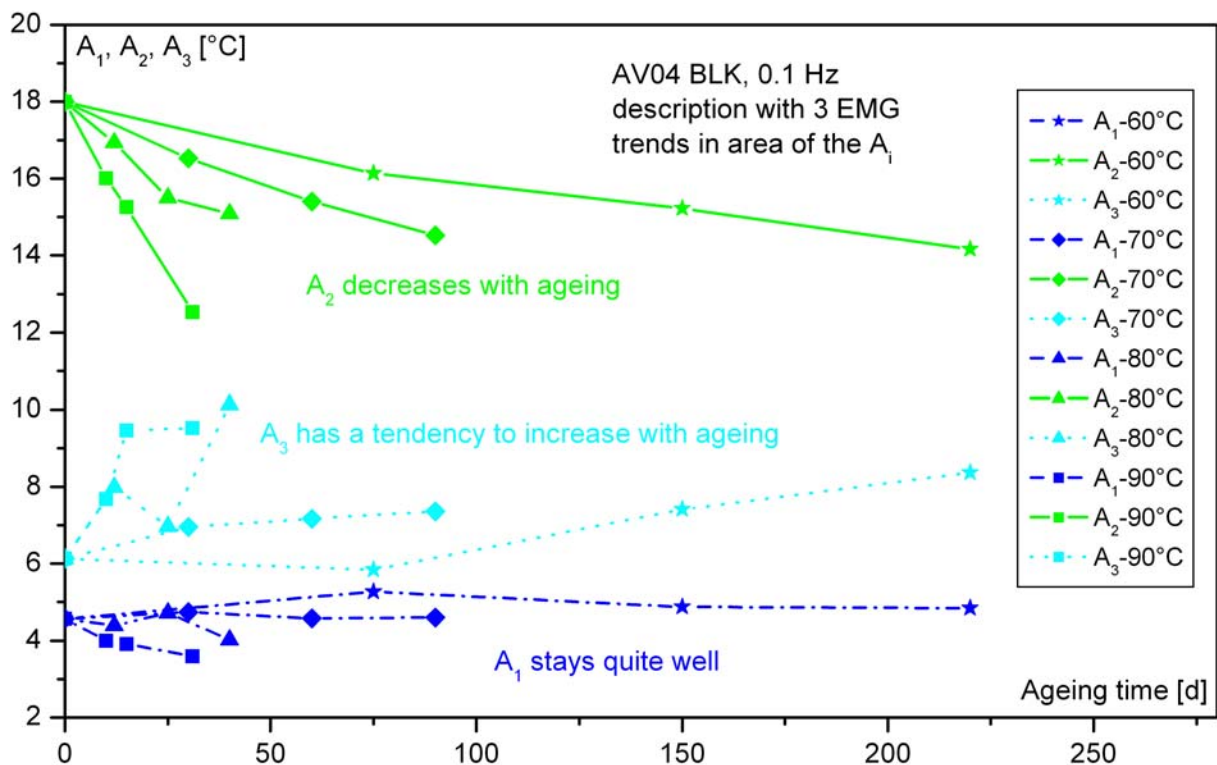

Figure 6: Trends of the peak areas with ageing time for the AV04 propellant.

By plotting the values of the peak areas versus the ageing times different tendencies can be underlined, see Fig. 6. The area A_1 of the first transition stays quite constant with ageing, whereas the other two show a tendency to increase (A_3) and to decrease (A_2) with ageing time. A linear dependence on ageing time is observed of these two last quantities at different ageing temperatures. By plotting the natural logarithm of the slopes $\ln(k_A)$ of these lines versus $1/T$ (temperature is in K) values of activation energies are obtained and compiled in Table 3.

$$ln(k_A) = ln(Z) - \frac{E_a}{R} \cdot \frac{1}{T} \qquad (7)$$

Because the areas Ai have the unit [°C] the decrease rates of them have the unit °C/time, here [°C·d^{-1}].

Table 3: Arrhenius parameters for rate constants of change of the peak areas A_2 and A_3 with ageing for the formulations AV03, AV04 and AV05.

propellant	transition 2 with area A_2			transition 3 with area A_3		
	Ea [kJ/mol]	log(Z [°C/d])	R^2	Ea [kJ/mol]	log(Z [°C/d])	R^2
AV03	70.1 ± 7	9.223 ± 0.96	0.9914	69.3 ± 6	9.128 ± 0.82	0.9873
AV04	77.8 ± 3	10.458 ± 0.44	0.9971	95.0 ± 10	12.769 ±1.48	0.9791
AV05	76.1 ± 5	10.356 ± 0.72	0.9921	72.3 ± 20	9.167 ± 3.00	0.8659

Some considerations can be done also for the values of the glass transition temperatures corresponding to the Gauss maxima temperatures of the peak transitions with the ageing time. The temperature characterising the first transition (Tc_1) stays quite constant with ageing, whereas the other two show a tendency to increase (Tc_2) or to decrease (Tc_3) with the ageing time.

3.2   Sol-Gel-Analysis

The interpretation of the sol fraction measurements in terms of cross-link density follows the approach of Charlesby and Pinner [7] to study the cross-linking of polymers due to radiation effects. Knowing S, the cross-linking density of the binder can be estimated following the modified version of the Charlesby-Pinner equation given for example in STANAG 4581 [8]. Because the propellant formulations are highly filled elastomers and because the cross-linking/chain scissioning of polymer chains influences only the binder network (pre-polymer and curing agent), the other components of the propellant formulations should not be taken into account, shown stepwise in the following. Eq. 8 shows the formula of the total soluble part with respect to the part of propellant without filler. With Eq. 9 the polymeric soluble part of the sample with respect to the polymeric part is determined.

$$S_{total} = \frac{E_{total}}{A_k} = \frac{E_{total}}{A \cdot (1 - P_{Al} - P_{AP})}. \qquad (8)$$

S_{total} = total soluble part of propellant with regard to A_k [-];
E_{total} = total amount of extract gained by the method [g];
A_k = corrected amount of A (A_k=A -A·P_{Al} -A·P_{AP}), this is the weighed-in amount
        without filler parts, correction is done by the nominal parts of Al and AP [g];
P_{Al} = nominal part of Al in composition (e.g., with 6 mass-% it is 0.06) [-];
P_{AP} = nominal part of AP in composition (e.g., with 72 mass-% it is 0.72) [-].

$$S_{poly} = \frac{E_{poly}}{A_{k-P}} = \frac{E_{total} - A \cdot P_{DOA} - A \cdot P_{AO}}{A \cdot (1 - P_{Al} - P_{AP} - P_{DOA} - P_{AO})}. \qquad (9)$$

S_{poly} = polymeric part of soluble part of composition with regard to A_{k-P} [-];
E_{poly} = polymeric part of total extract, corrected by nominal parts of plasticiser
        and AO [g];
A_{k-P} = corrected amount of A, correction done by the nominal parts of not considered
        components Al, AP, DOA, AO and if necessary other components [g];
P_{DOA} = nominal part of DOA in composition (with 4 mass-% it is 0.04) [-];
P_{AO} = nominal part of AO in composition (with 0.2 mass-% it is 0.002) [-].

Table 4 shows the difference in the soluble fraction values considering the different soluble fractions: S_{prop} (Eq.1), S_{total} (Eq. 8), S_{poly} (Eq. 9).

Table 4: Comparison of the soluble fraction values obtained with three different evaluation methods (S_{prop}, S_{total}, S_{poly}) of the AV06 propellant formulation.

Ageing temperature [°C]	Ageing time [days]	S_{prop} [-]	S_{total} [-]	S_{poly} [-]
25	0	0.066192	0.413699	0.205016
70	60	0.059004	0.368774	0.144100
	90	0.058528	0.365797	0.140064
	120	0.053534	0.334585	0.097742
80	25	0.061420	0.383873	0.164574
	40	0.056156	0.350974	0.119964
	50	0.052514	0.328216	0.089106
90	10	0.057970	0.362311	0.135338
	15	0.054609	0.341307	0.106857
	20	0.052930	0.330815	0.092630

S_{poly} was the parameter used for the evaluation of the cross-link density C, a dimensionless quantity, see Eq.(10).

$$C = \frac{\left(1 - S_{poly}\right) \cdot \left(2 - \left(S_{poly} + \sqrt{S_{poly}}\right)\right)}{\left(S_{poly} + \sqrt{S_{poly}}\right)} \tag{10}$$

By plotting $C = f(S_{type})$ the graph in Fig. 7 can be obtained. A soluble fraction equal 1 means that the material is not cured and that all can be extracted. In contrast, a value of S_{type} tending to 0 means that nothing can be extracted. For a propellant formulation, the soluble fraction S_{poly} should be in the range 0.15 to 0.2 to get an elastomer with low cross-link density to achieve a suitable rubbery state.
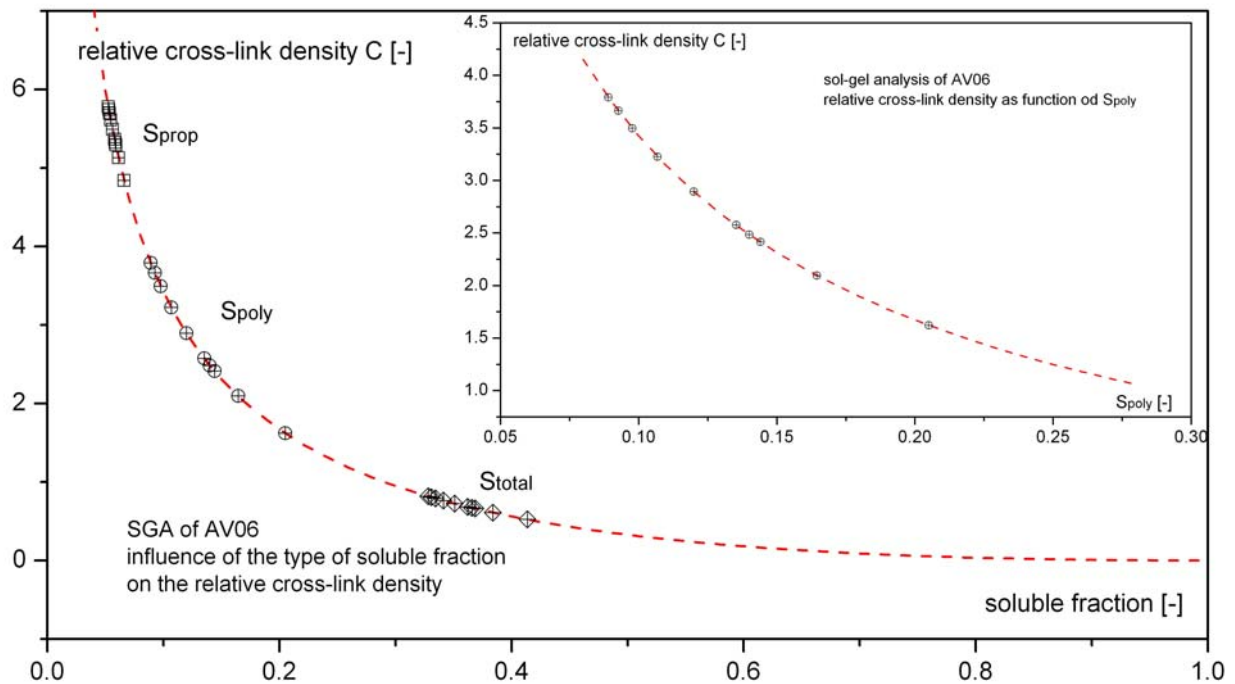

Figure 7: Cross-link density C versus S_{prop}, S_{total} and S_{poly} of the AV06 propellant formulation. The figure insert shows C only as function of S_{poly}.
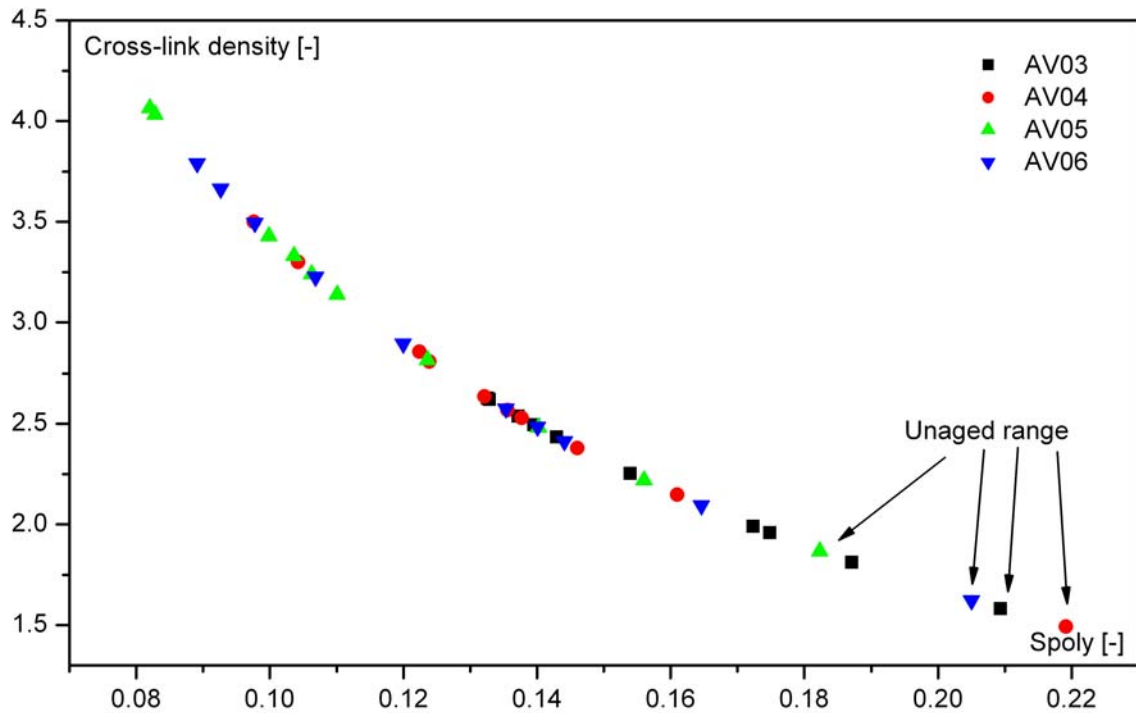
Figure 8: Cross-link density C vs. S_{poly} of all investigated AV0x propellant formulations.

Fig. 8 shows also the values of the unaged propellant formulations. The formulations containing only micrometric aluminium (AV03, AV04) have the higher soluble fraction values, whereas the formulation containing a part (AV06) or only nanometric aluminium (AV05) are characterised by lower S_{poly} content and therefore higher formal cross-link density values. By plotting all the values (unaged and aged) together the trend with ageing can be followed in Fig. 8. All the AV0x propellant formulations evidence an increase in the cross-link density values with ageing. This implies that the oxidative cross-linking is more effective than the chain scission.
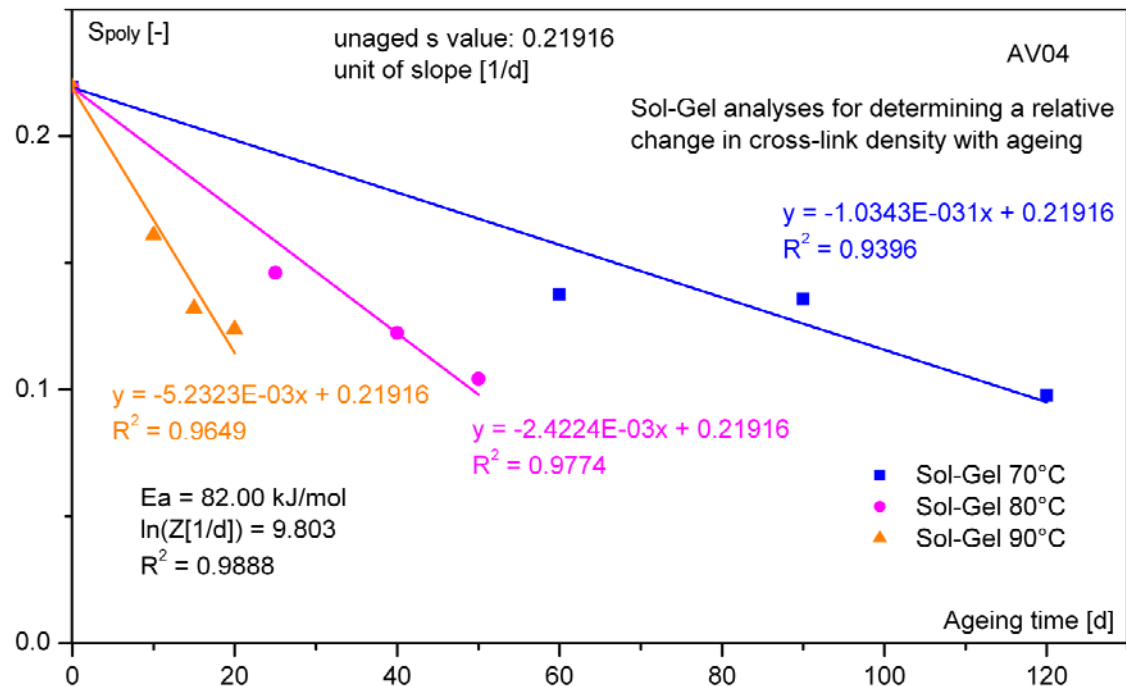

Figure 9: Effect of time and temperature on the soluble fraction of the AV04 propellant.

The amount of soluble fraction obtained is ageing time and ageing temperature dependent. Making a linear interpolation of the temperature grouped values and fixing the initial value

$S_{poly}(0)$ equal to the unaged S_{poly}, the slopes $k_S(T)$ of the straight lines at different ageing temperatures are obtained, see Fig. 9. The implied modelling is in terms of kinetics given in the following equations 11 and 12. Formally, the data decrease according to a reaction of zero order with a rate constant k_S.

$$\left(\frac{dS_{poly}(t,T)}{dt}\right)\Bigg|_T = -k_S(T) = -Z_S \cdot \exp\left(-\frac{Ea_S}{RT}\right) \tag{11}$$

$$S_{poly}(t,T) = S_{poly}(0) - k_S(T) \cdot t \tag{12}$$

By plotting the natural logarithm of the slopes $\ln(k_S)$ versus $1/T$ (temperature in K) the values of the Arrhenius parameters of k_S are obtained and compiled in Table 5.

Table 5: Arrhenius parameters for rate constants k_S of change of the soluble fraction S_{poly} of the investigated propellant formulations.

	AV03	AV04	AV05	AV06
Ea_S [kJ/mol]	85.1 ± 3	84.0 ± 1	72.3 ± 3	101.5 ± 5
$\log(Z_S$ [1/d])	9.794 ± 0.42	9.803 ± 0.10	7.967 ± 0.35	12.373 ± 0.74
R^2	0.9989	0.9998	0.9989	0.9976

By the way, all three types of soluble fraction S_{type} give the same activation energies, only the Z factors differ.
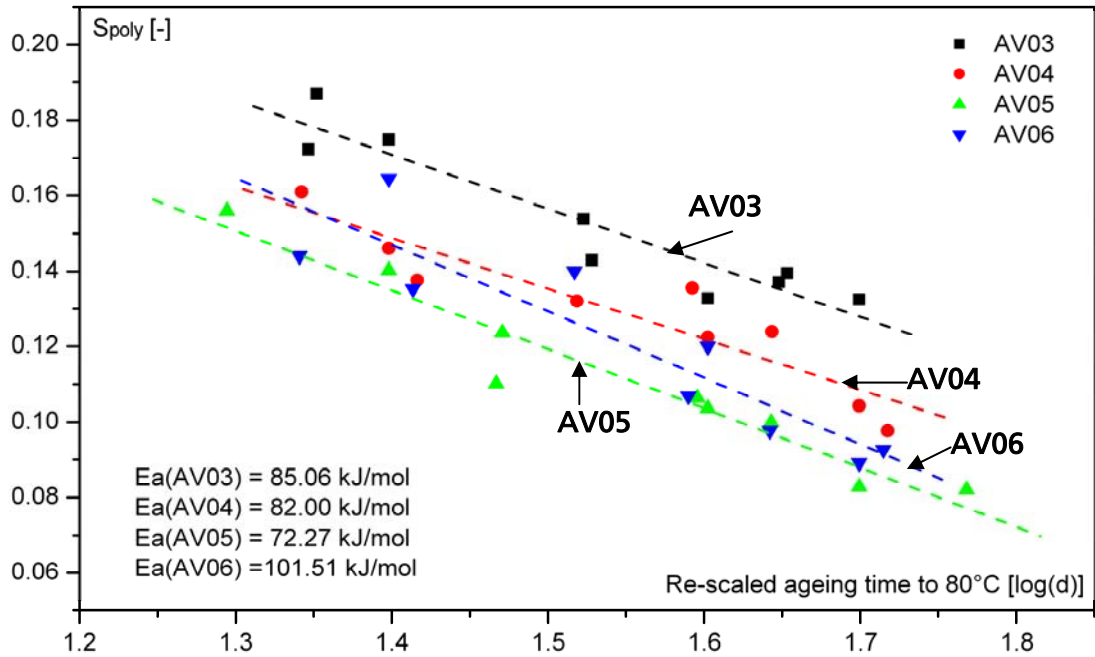

Figure 10: Decrease of S_{poly} with the re-scaled ageing times (shown in logarithmic scale) to 80°C (t_E) for the investigated formulations.

With Eq. 13 it is possible to scale the test time t_T to any target time t_E using the test temperature T_T and the target temperature T_E.

$$t_E = t_T \cdot \exp\left(\frac{E_a}{R} \cdot \left(\frac{1}{T_E} - \frac{1}{T_T}\right)\right) \tag{13}$$

Considering $T_E=80°C$ and as T_T and t_T the ageing temperature and ageing time for the aged samples the soluble fraction of the aged propellant formulations have been plotted as function of the ageing time t_E re-scaled to $T_E = 80°C$. A linear interpolation of the data in logarithmic time scale can be applied as shown in Fig. 10. Propellants containing microAl show high solu-

ble fraction values with respect to the corresponding formulations containing only nanoAl or a fraction of nanoAl. The slopes of the straight lines belonging to the formulations which have nanoAl is higher, indicating a faster decrease of the sol fraction with time or, respectively, a faster increase of the cross-link density.

3.3   GPC analysis of propellant extracts

The Fig. 11 shows typical GPC elugrams obtained and some elugrams of the ingredients DOA and Irganox 565. One can see that the peaks at the end, means at higher elution volumes Ve, can be identified as DOA and Irganox by injecting solutions containing them alone. Further to see are the uncured pre-polymer HTPB R45M^{TM} and two elugrams of the extracts of formulation AV04, obtained from unaged material and material aged at 90°C over 20 days. Clearly to see is that the unaged material and also the aged one is higher in mean molar mass than HTPB R45M^{TM}, the elugrams start at much lower elution volumes Ve means at much higher molar mass M. This can be seen directly in Fig. 12, which shows the corresponding molar mass distribution (MMD) functions. The mean molar mass Mn of the unaged AV04 is 2.3 fold of the one of HTPB. This means chain extension by addition of IPDI and about one further HTPB chain has happened in average. The extracted intermediate long chains have been not cross-linked to the binder network. After ageing at 90°C over 20 days the mean molar masses are smaller. In average the chains are still longer by a factor of 1.65 than in HTPB. From Fig. 12 one recognises that the distribution has narrowed compared to the one of the unaged material. This indicates that the longer chains are cross-linked to the binder with higher probability than the shorter ones. Fig. 13 and Fig. 14 show the complete series of MMD for AV03 and AV04 aged at 90°C. An increase on the low molecular side of the MMD indicates now directly experimentally that also chain scission happens.
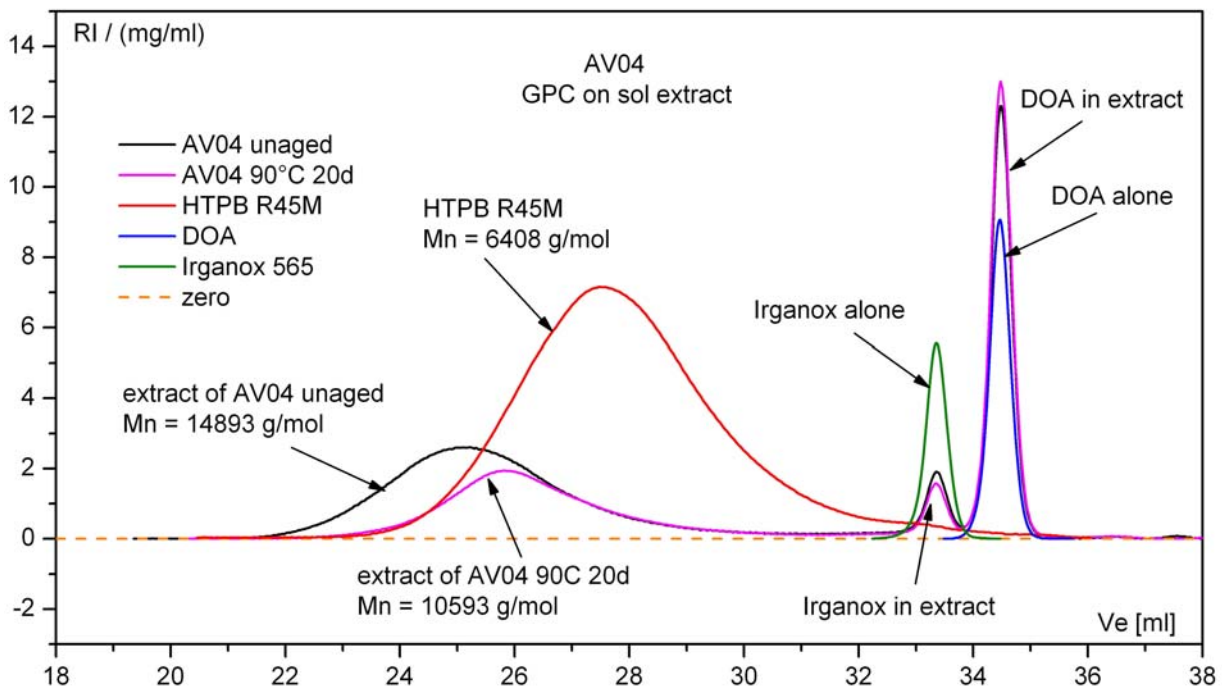

Figure 11: Elugrams of extracts of AV04, of HTPB R45M^{TM} and of plasticiser DOA and anti-oxidant Irganox 565.
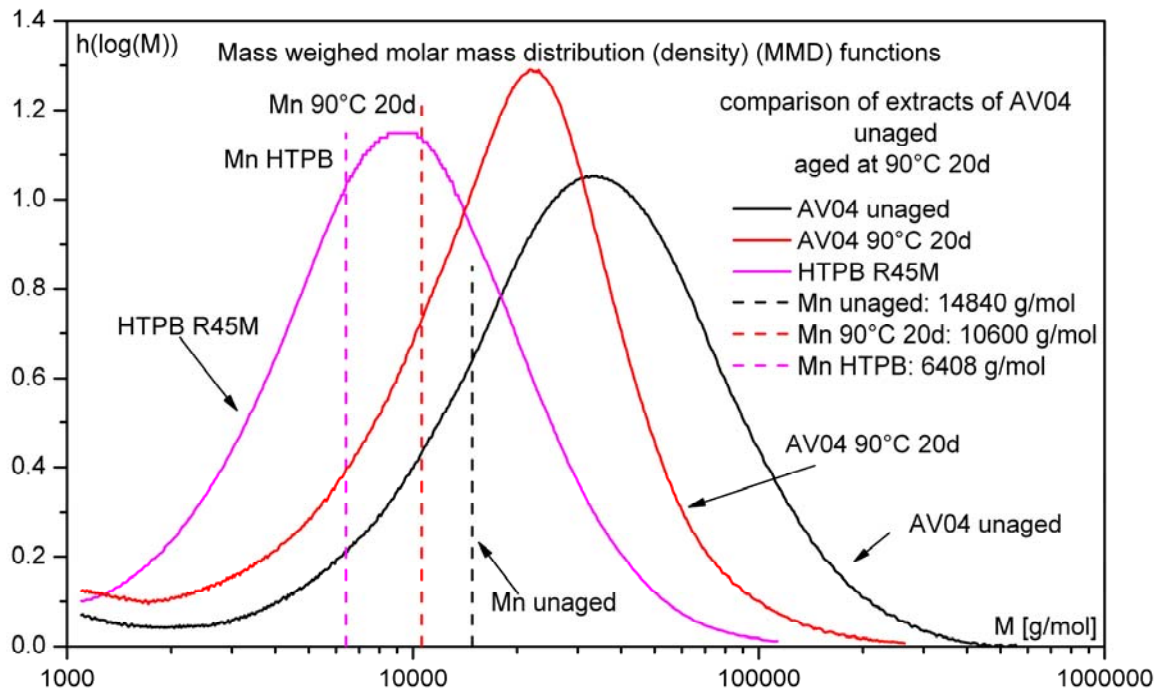
Figure 12: Molar mass distribution functions of two extracts from AV04 and of HTPB R45M^{TM}.
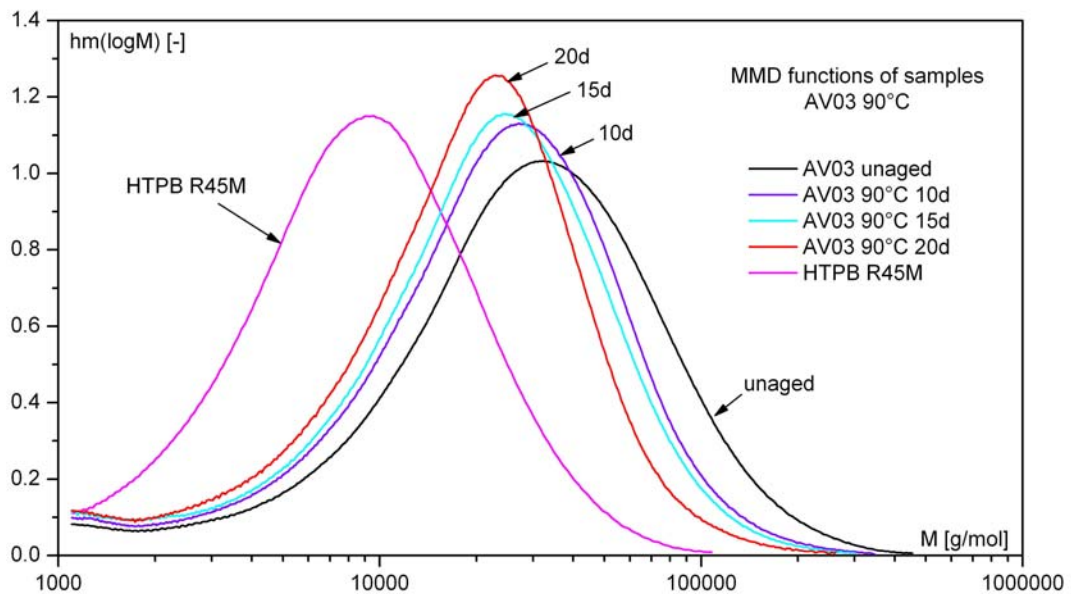

Figure 13: Molar mass distribution functions of the complete series of AV03 and of HTPB R45M^{TM}.
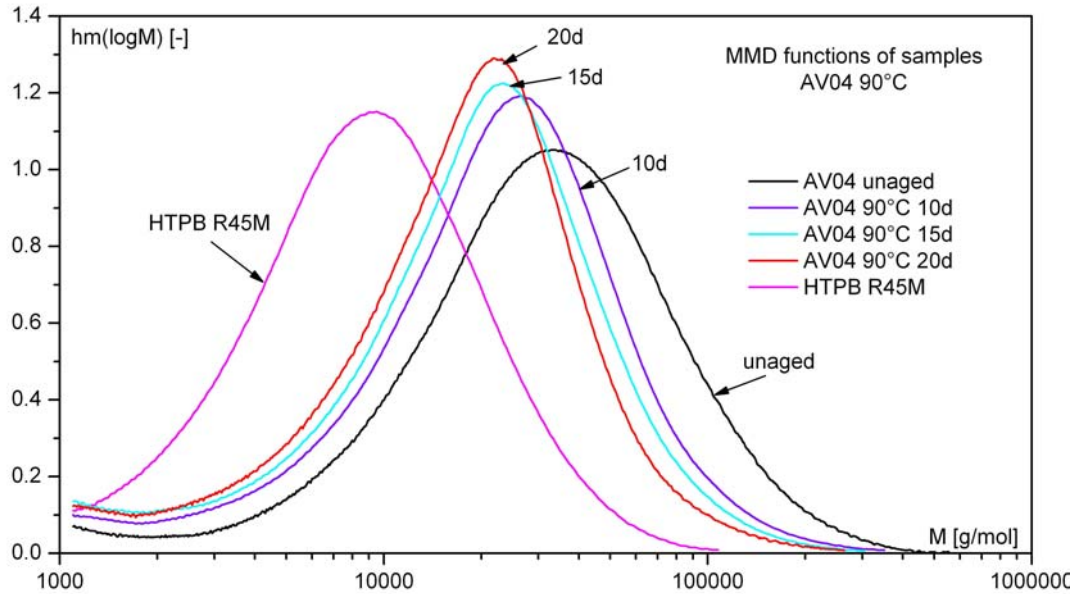
Figure 14: Molar mass distribution functions of the complete series of AV04 and of HTPB R45M[TM].

The change with ageing of the Irganox content and of the concentration normalised polymer eluate area are shown in Fig. 15. With concentration normalised polymer eluate area EAn the eluate area of the polymer part is meant, divided by the concentration value of the extract solution used for the GPC analysis. Both quantities decrease. This means the antioxidant is consumed and the amount of extractable polymeric part decreases with ageing. The latter quantity indicates that during ageing some of the free chains are bonded to the binder network. If this would not happen, the eluate area should stay constant. Consumption of Irganox indicates the activity of oxygen in the sample. Because DOA content does not change in the propellant by reaction (evaporation is possible, under high humidity a hydrolysis could occur), it shows a pseudo increase in concentration in the extracted part.
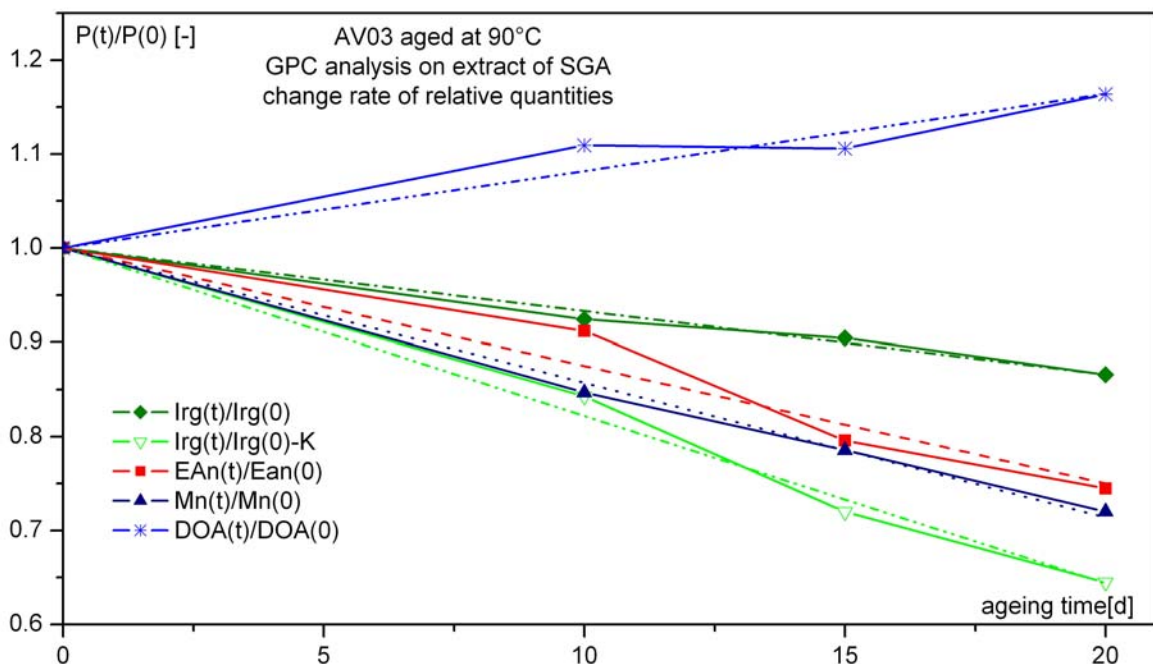

Figure 15: Change of initial value normalised quantities with ageing at 90°C in AV03. Decrease of antioxidant Irganox 565 and of the concentration normalized polymer eluate area

EAn of AV03. The content of plasticiser DOA increases because of decreasing polymer content. The Irganox-K content is corrected for the pseudo-increase by decreasing polymer content.
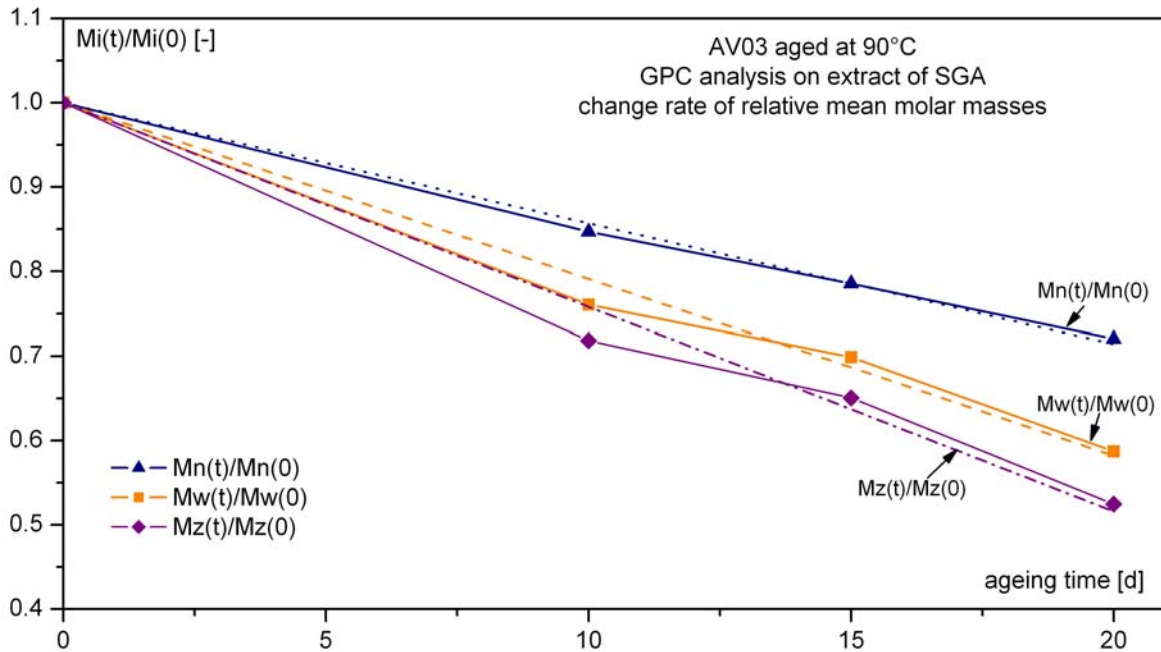

Figure 16: Decrease of initial value normalised mean molar masses Mn, Mw and Mz at 90°C of AV03.

Further to see are the relative (=initial value normalised) mean molar mass Mn and a corrected Irganox content. Here this pseudo increase in concentration by decreasing polymer content was taken out from the real measurement values. The decrease in relative mean molar masses Mn, Mw and Mz is presented in Fig. 16. From the temperature dependence of the rate constants the Arrhenius parameterisation is obtained, see Table 6 and Table 7. In determination of the rate constants of a property P a just linear change with time was assumed, formulated in the Equations 14 and 15. Initial value normalized $P_{rel}(t) = P(t)/P(0)$ is used.

$$\left(\frac{dP_{rel}(t,T)}{dt}\right)\bigg|_T = S \cdot k_P(T) = S \cdot Z_p \cdot \exp\left(-\frac{Ea_P}{RT}\right) \tag{14}$$

$$P_{rel}(t,T) = P_{rel}(0) + S \cdot k_P(T) \cdot t \tag{15}$$

The parameter S is a sign parameter and is -1 for decreasing properties with time and +1 for increasing properties with time. $P_{rel}(0)$ is 1 by correct normalization.

Table 6: Rate constants $dP(t)_{rel}/dt$ in 1/d of change of quantity $P_{rel}(t) = P(t)/P(0)$ with ageing for RP formulation AV03. The minus sign indicates a decrease in values; the plus sign indicates an increase in values. Only the content of DOA shows an increase, but because of decrease in polymer part in extract. Unit of Mn(0), Mw(0) and Mz(0) is $g \cdot mol^{-1}$.

|	Mn_{rel}	Mw_{rel}	Mz_{rel}	EAn_{rel}	Irg_{rel}	Irg_{rel-K}	DOA_{rel}
80°C	-6.193 E-3	-8.334 E-3	-9.744 E-3	-5.439 E-3	-3.257 E-3	-1.776E-2	8.218E-3
85°C	-9.691 E-3	-1.325 E-2	-1.498 E-2	-6.944 E-3	-3.888 E-3	-1.012E-2	6.531E-3
90°C	-1.427 E-2	-2.093 E-2	-2.423 E-2	-1.248 E-2	-6.715 E-3	-7.921E-3	3.903E-3
	Mn(0)	Mw(0)	Mz(0)	EAn(0)	Irg(0)	Irg(0)	DOA(0)
P(0) val.	15217	42311	84239	10.076 au	2.54 m.-%	2.54 m.-%	56.71 m.-%

Table 7: Arrhenius parameters for rate constants of change k_P of quantity $P_{rel}(t) = P(t)/P(0)$ with ageing for RP formulation AV03.

	Mn_{rel}	Mw_{rel}	Mz_{rel}	EAn_{rel}	Irg_{rel}	Irg_{rel-K}	DOA_{rel}
Ea_P [kJ·mol^{-1}]	89.0 ± 3	98.2 ± 0.4	97.1 ± 4	88.4 ± 22	77.0 ± 23	85.9 ± 20	79.5 ± 17
$lg(Z_P$ [d^{-1}])	10.958 ± 0.45	12.440 ± 0.06	12.345 ± 0.57	10.787 ± 3.18	8.870 ± 3.41	10.585 ± 2.95	9.376 ± 2.47
R^2	0.9988	0.9999	0.9984	0.9428	0.9156	0.9476	0.9568

Table 8: Change rates k_P in 1/d for the decrease with ageing time of initial value normalized properties P_{rel} at 90°C.

	Mn(t)/Mn(0)	Mw(t)/Mw(0)	Mz(t)/Mz(0)		EAn(t)/EAn(0)	Irg(t)/Irg(0)-K
AV03	1.427E-02	2.093E-02	2.423E-02		1.248E-02	1.776E-02
AV04	1.364E-02	2.343E-02	2.499E-02		1.746E-02	2.245E-02
AV06	1.904E-02	2.419E-02	2.596E-02		1.718E-02	2.172E-02

In Table 8 the change rates of some initial value normalised quantities at 90°C for three propellant formulations are given. The graphical presentation in Fig. 17 shows that in average the change rates are highest for AV06 and lowest for AV03.
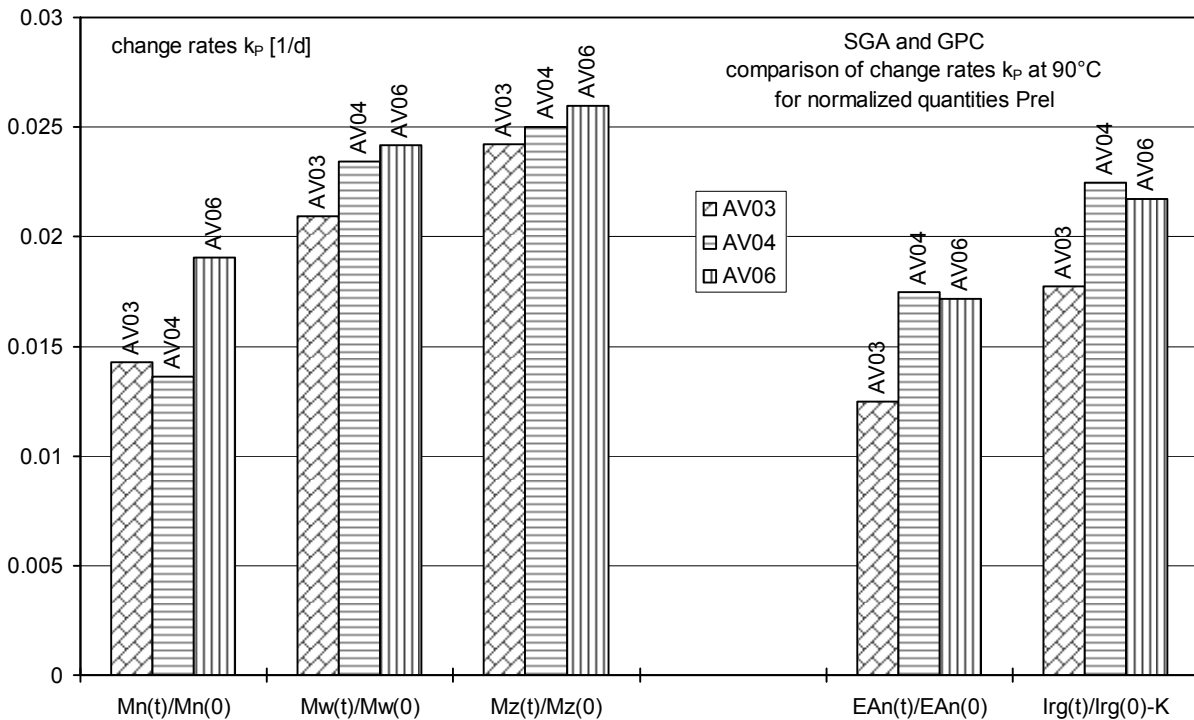
Fig. 17: Comparison of change rates k_P at 90°C for properties Prel of three formulations.

3.4 SEM measurements

Some picture of the propellant specimens before and after the Soxhlet analyses were taken with the SEM. Fig. 18 shows the swelling behaviour of a propellant sample swollen in toluene. The picture was taken immediately after the removal from the solvent. The weight and the volume is about twice the unswollen sample. With so small samples the DLO effects are significantly reduced (no strong gradient in the oxidative ageing) and the diffusion of the solvent can

be considered as homogeneous in the entire specimen. Fig. 19 gives a schematic representation of the swelling of a propellant specimen. When the material is dipped in a solvent, the liquid penetrates the cured material. The distance between the free chains, filler particles and in the network increases due to the presence of the solvent, the volume of the specimen is bigger and the material is under a stretched condition (isotropic constitutive behaviour).
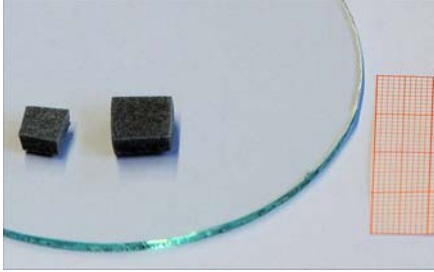

Figure 18: Swelling of the binder after the extraction with toluene. Left: unswollen specimen before the solvent extraction. Right: swollen sample.
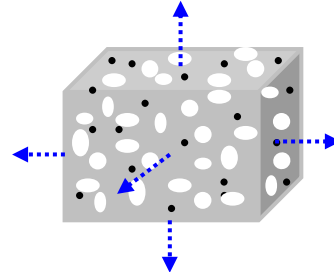

Figure 19: Schematic representation of the swelling of a propellant specimen.

The SEM micrographs underline the difference between the samples before (Fig. 21) and after (Fig. 20) the Soxhlet and desiccation processes. The samples belong to two different formulations: AV03 and AV05. Anyway, both the samples were cut with a scalpel and can be defined as unstressed materials. While the surface of the AV05 propellant is flat (Fig. 21), AV03 displays a "3D" surface; the AP particles seem to be on the surface due to the swelling. The dewetting of the particles is evident (Fig. 20). This material shows a powdery aspect, the oxidiser particles seem to be dug around. Moreover, the scratch resistance of extracted AV03 is extremely low, for example, the AP particles could be removed easily with a spatula or even by finger nail.
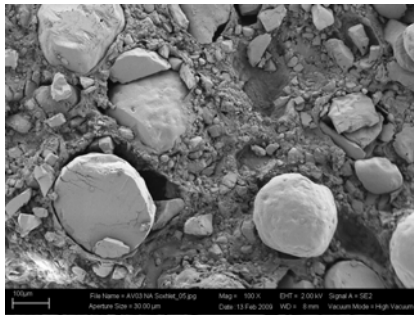

Figure 20: SEM image of the AV03 propellant after the solvent extraction at small magnification.
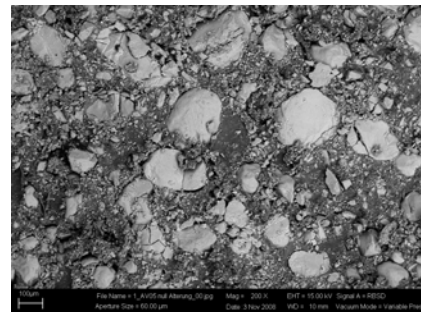

Figure 21: SEM image of the unstressed AV05 propellant at small magnification.

4   Discussions

4.1   DMA

The values of $\tan(\delta)$ describe the balance between the viscous and elastic behaviours as can be seen in Table 9. A molecular interpretation of the viscoleastic behaviour can be given considering the loss factor and the glass transition temperature. The term glass transition defines a temperature induced transition region of an amorphous polymer phase from its energy-elastic to its entropy-elastic state und vice versa. The reason for this transition is to reach always an energetic minimum, here that of the Gibbs free enthalpy, Eq. 16:

$$\Delta G(p,T) = \Delta H(p,T) - T \cdot \Delta S(p,T) \,. \tag{16}$$

In the energy-elastic state the internal energy is controlled by lattice like energetic interactions between the polymer molecules. The enthalpy term ΔH controls the Gibbs free enthalpy ΔG. Because of lower temperatures the distances between the polymer chain elements are small, mobility is restricted and local dipole-dipole interaction has a strong effect in lowering internal energy: ΔH becomes appreciably negative and the entropy term plays nearly no role, because there is little change in configuration of the polymer chains. In the energy-elastic state the entropy term is significantly smaller than the enthalpy term. In contrast, in the entropy-elastic state the internal energy is not controlled by lattice like energetic interactions between the polymer molecules. The increase in available free volume at higher temperatures gives them more possibilities to realize many configurations, means that the entropy is increased. The term $T \cdot \Delta S$ in Eq. 16 gets more positive and ΔG gets more negative and the entropy term $T \cdot \Delta S$ controls now the Gibbs free enthalpy ΔG. The enthalpy ΔH increases, means is less negative than in energy-elastic state. It plays now nearly no role, because its value varies only a little with changing temperature above the glass transition. The distances between the chain elements increase. Local dipole-dipole-interactions are less effective because of averaging out by the thermal movements of the chain elements. Any effect that reduces the possibility of realisation of configurations of the polymer chains (presence of filler and binder/filler interactions) will reduce the entropy part and increase the enthalpy part making the material less entropy elastic and strain capacity should become smaller.

Table 9: Values of tan(δ) at some phase angles and assignments of qualitative meanings.

tan(δ)	Description	δ	Qualitative meaning
0	Ideal elastic	0°	Solid without any dissipation of applied deformation energy
0.176	Visco-elastic	10°	Solid with frictional dissipation, no molecular rearrangement
0.364	Visco-elastic	20°	Polymer, some elastic behaviour and frictional energy dissipation
0.577	Visco-elastic	30°	Polymer, rearrangement of molecules
1	Visco-elastic	45°	Polymer, rearrangement of molecules
3	Viscous	71°	Melting polymer, residual energy storage
10	Viscous	85°	Melting polymer
∞	Ideally viscous = totally dissipative	90°	Liquid (low to medium large molecules), no elastic energy storage possible

The loss factor tan(δ) is a composed distribution function (non-normalised density function) describing the distributions of the glass transitions of the structural elements of the polymer network in propellant formulations. The first maximum, also called main peak, is associated with the glass transition of the HTPB main chain elements (soft-segment units) where the main chain molecular motion ceases or starts, the temperature corresponding to the maximum of the peak is called $T_g^{unrestricted}$. The second peak is related to the motions around the short hard-segment units (urethane groups) and/or mobility restricted soft-segment regions, caused by the presence of filler particles and by binder/filler interactions. In order to point out the restriction the temperature corresponding to the maximum of the second peak was named as $T_g^{restricted}$.

The values describing the first peak (loss factor part and $T_g^{unrestricted}$) do not change with the ageing time, whereas the values of tan(δ) of the second peak and $T_g^{restricted}$ (Fig. 3) decrease with the ageing time, also the area under the peaks is reduced. This can be interpreted in terms of more mobility restriction, means of forming a so-named rigid amorphous phase, which is not able or less able to perform the glass transition. The evolution of the loss factor has not only one reason but during the radical based oxidative ageing two competitive processes take

place: chain scission and intermolecular chain radical combination thereby forming cross-linking. A decrease of tan(δ) means the formation of more cross-linked and therefore more rigid three-dimensional network. An increase of tan(δ) characterises an increase of the macromolecular mobility, which can be caused by chain scission [9] and/or by dewetting between binder and filler particles [10].

An interpretation of the three transition regions found is tried in the following. For this we consider first the loss factor curve and its description with three EMGs of the binder alone, consisting of HTPB-IPDI network, 25 mass-% plasticiser DOA and 1.09 mass-% Irganox 565, named as AV00, see Figure 22. The apparent main transition peak of the binder is composed of two sub-regions, one situated slightly at lower temperatures. From the determined parameters one recognises that the exponential decay parts are quite low especially for one of the main transitions. This reflects the undisturbed situation, only little frictional movement parts are present. At higher temperatures around -30°C, a third transition appears, which is broad but still well symmetrical. This third transition is assigned to restricted chain mobility caused by the urethane linked isophorone units. Because the OH number per HTPB chain is in average 2.2 there is the possibility of multiple urethanes cross-linking per chain, which are also statistically distributed. This enhances mobility restriction of the HTPB chain. Figure 23 shows the extent of the effect of 25 mass-% DOA in the HTPB-IPDI polymeric network. The main transition is shifted to lower temperatures and its peak height increases significantly. This can be seen as a general reduction of mobility restrictions or the increase of free volume for the HTPB chains. The pure HTPB-IPDI shows only a faint second transition; this means the mobility restrictions around the urethane cross-linking sites are quite high and in part rigid. Also here one has a shift to lower temperatures and an increase of the transition peak by addition of DOA, means some increase in molecular mobility (= free volume).

In Figure 24 the comparison between unaged AV00 and unaged AV04 at 0.1 Hz deformation frequency is made. The main effect of the fillers AP and Al particles is a strong general mobility restriction for the binder evidenced by the strong decrease of the main transition peak of the binder. The two sub-transitions of the binder main transition are still present. One is nearly not shifted but less in intensity. The other is shifted to higher temperatures (from about -75°C to around -66°C) because of the reduction in free volume and mobility reduction because of additional fixations along the HTPB chains. These fixations are at least threefold in type: the bonding agent HX 878 is a so-named active one. It contacts AP particles via ionic bonds and is bonded to the network via urethane links with IPDI. The OH part of HX 878 is considered in the adjusted NCO/OH ratio. HX 878 is a very 'condensed' molecule, means the mobility restriction caused by it are relatively high. The Al particles must be considered as so-named active fillers, means because of a lot of interaction sites on their surface the HTPB chain mobility is again restricted. This is realised by dispersive (van der Waals) interaction with the double bond of HTPB and because of possible IPDI bonding via OH-groups at the Al particle surface, see also later. An estimation of this dispersion interaction provides with interaction energies in the range of the found activation energies. The peak range around -25°C appears enhanced in the filled system compared to the binder alone. This may be explained by the free extended HTPB chains (found with GPC) intermixed in the urethane cross-linking regions and in this way creating more free volume in these regions compared to the binder alone. The part of these free chains should be higher in AV0x than in the pure binder, because of migration hindrance by the fillers in encountering 'open' reactive ends and because of consumption of IPDI by Al particles, see below. In addition, the squeezing in of filler particles by the kneading process into the urethane-restricted ranges breaks up some of the interactions which caused mobility restrictions.

As already discussed, by ageing we have several competitive effects on the loss factor curves. First to say, during ageing we have seen a very small loss in plasticiser. In considering the effect of DOA on the peak position and peak size changes in the binder, Figure 23, one can conclude that the small loss of about 0.2 mass-% of the propellant could correspond to a loss of 1.3 mass-% from 25 mass-% of DOA, means a relative plasticiser loss around 5 %. How-

ever, the thereby induced effect must be qualitatively equal on all transition peaks. This is not the case, see Table A1 in [20]. Plasticiser loss should shift all peaks to higher temperatures. Only peak 2 is recognizably shifted to higher temperatures. The others stay constant or show tendencies to lower temperatures. From this it is concluded that plasticiser loss is not an applicable explanation for the observed changes. A complete explanation must take into account all the changes in the transition ranges: the peak area, the peak width, the peak position and the relaxation part of the peaks, see Appendix 3 in [20]. The residual main chain transition peak 1 stays nearly unchanged; a slight shift to lower temperatures appears to be possible. For the third peak around -66°C the changes are significant. The peak area A_3 increases, the relaxation part increases, the widths w_3 stays constant with tendency to decrease and the peak temperature Tc_3 decreases, whereby the EMG peak temperature Tp_3 stays more or less constant. The second peak around -26°C changes also significantly. The peak area A_2 decreases, the widths w_2 stay constant with tendency to decrease, the relaxation part decreases somewhat and the peak temperature Tc_2 decreases. The EMG peak temperature Tp_2 decrease also, but less in extent than Tc_2.
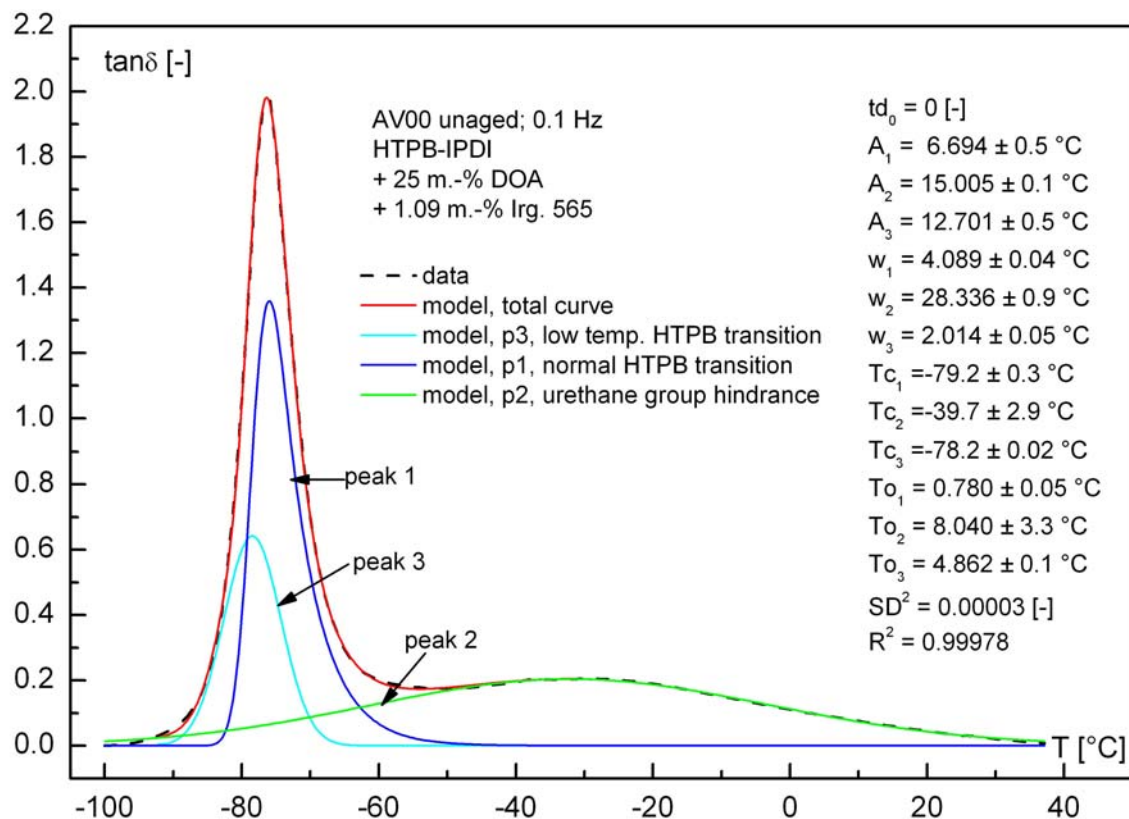

Figure 22: Loss factor curve of unaged binder HTPB with plasticiser and Irganox, named AV00. Shown is the modelling with three EMG functions. Two transitions constitute the main transition peak, and one transition at around -30°C represents a restricted mobility region, which could be caused by isophorone-urethane groups.

Increasing transition intensity of peak 3 indicates increase in free volume or less mobility restriction by the above discussed interactions between particles and binder chains. Also chain splitting could help to lower interaction restrictions. The active Al particle surface can help in oxidative chain splitting and thus lowering the interaction. In addition, surface modifications of the Al particles should be taken into consideration. Residual water can support the dissolving of the bonding agent from the AP surface. For peak 2 the observed free chains by GPC and their scission during ageing and cross-linking to the binder reduces the effect of creating free volume in the urethane bonding regions.
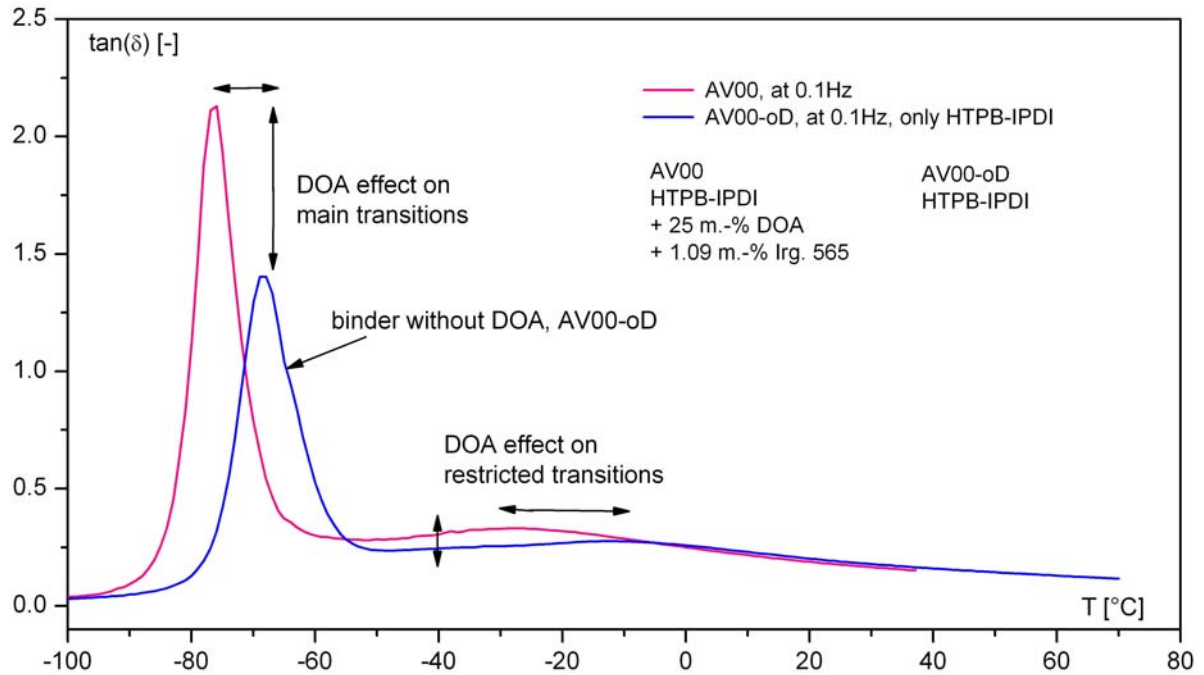
Figure 23: Comparison of loss factor curves of unfilled binder containing plasticiser and AO with the pure polymer network of HTPB-IPDI.
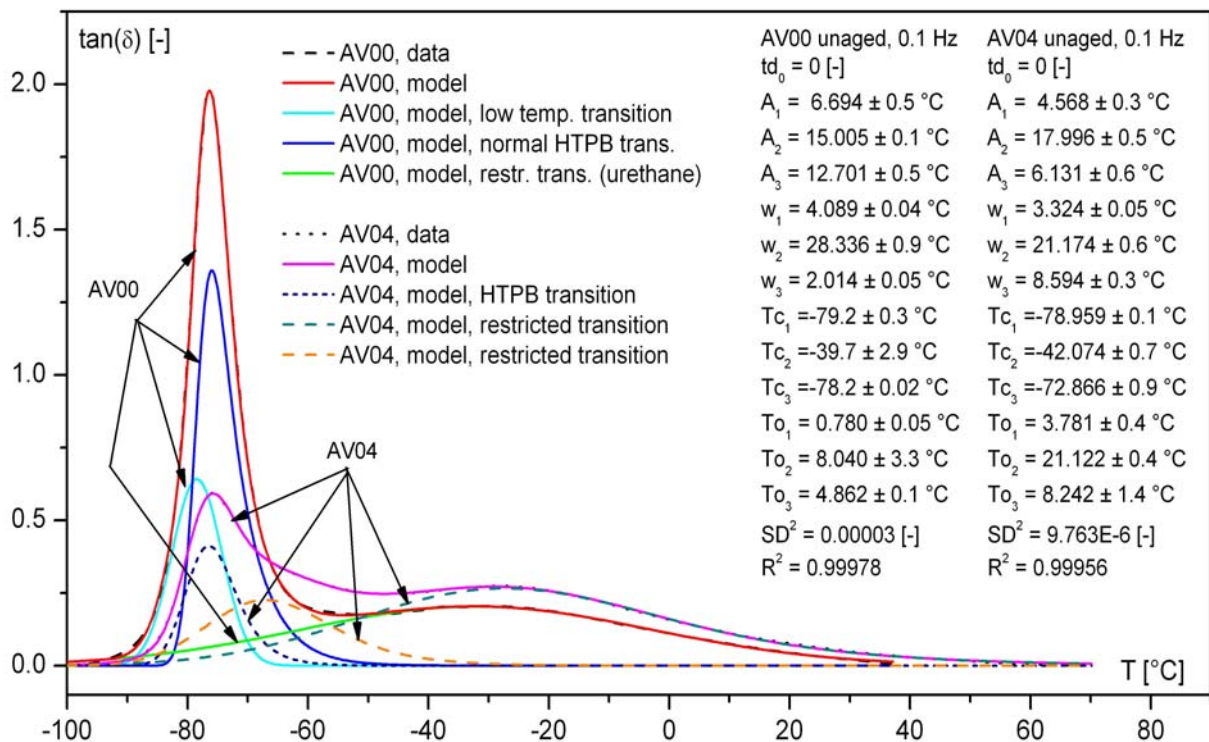

Figure 24: Comparison of loss factor curves of unaged binder HTPB with plasticiser and Irganox 565 and of unaged formulation AV04. Both curves are described by three EMGs.

This leads to a more rigid phase, and this in turn leads to reduction in loss factor intensity or area A_2 and in slight shifting to higher temperatures. A further effect can be the following phenomena. Debonding or already weakening between binder and AP and /or Al particles cause an increase in free volume and thereby a shift of the corresponding transition region to lower

temperatures, inducing there an increase in transition intensity, but in the range of peak 2 reduction of it. Another possibility of chain movement is a coordinated long segment movement known also as reptation behaviour [17], means a snake-type movement, which will be enabled at higher temperatures. This chain segments may disappear by chain scission or by cross-linking and the corresponding area A_2 in loss factor will decrease. Shorter chain segments gain in mobility and appear at lower temperature. Seen all together several explanation aspects are possible to explain the observed behaviour and may be several of the discussed mechanisms could happen.

In Table 10 the peak areas of the three EMG functions describing the loss factor curves of AV00 and AV04 have been compiled and some ratios have been formed for illustrating the changes in relative transition intensities. The total peak area is in unfilled state 20% higher. With regard to the main transition composed of two sub-peaks AV00 is 80% higher in area. The restricted second peak gains intensity by filling the binder.

Table 10: Comparison of formulations A00 (unfilled binder) and AV04 by the EMG peak areas.

EMG peak area	AV00	AV04	AV00	AV04	AV00	AV04	AV00	AV04	AV00	AV04
A_1 [°C]	6.69	4.57	6.69	4.57	6.69	4.57				
A_2 [°C]	15.01	18.00							15.01	18.00
A_3 [°C]	12.70	6.13	12.70	6.13			12.70	6.13		
Sum [°C]	34.40	28.70	19.39	10.70						
Area ratio AV00 to AV04	1.20		1,81		1.46		2.07		0.83	
Area meaning	total area		unrestricted area A_1 +A_3		unrestricted area A_1		unrestricted area A_3		restricted area A_2	

4.2 SGA

By comparing the formulations having micrometric Al inside it is evident that the one having more Al inside (12 mass-%) and therefore less AP has a higher soluble fraction, see Table 11. This can be explained recalling that the formulations contain 0.19 mass-% of bonding agent HX-878. The bonding agent is a material which produces an interaction between the oxidiser crystals and the binder by forming a primary chemical bond (through the –OH group reactive with the curing agent) and on the other side an ionic bond with the oxidiser particle by replacing ammonia. Hence, the absence of 6 mass-% of AP for AV04 can explain the lower value of the cross-link density. However, this consideration cannot be used for the AV05 and AV06 formulations, because each of them has the same AP mass fraction as the corresponding micrometric formulations AV03 and AV04. The only difference between these two groups is the presence of nanoAl. Also previous results [5] obtained with the tensile tests have evidenced a different behaviour (reinforcing effect) of the material having nanoAl inside.

Table 11: Soluble fraction and cross-link values of the unaged propellant formulations.

Formulations	AP [m.-%]	µ-Al [m.-%]	n-Al [m.-%]	Soluble fraction [-]	Cross-link-density [-]
AV03	78	6	-	0.209309	1.580971
AV04	72	12	-	0.219160	1.491706
AV05	78	-	6	0.182331	1.866539
AV06	72	6	6	0.205016	1.622119

The behaviour of the AV05 and AV06 propellants can be explained by considering results obtained with rigid polyurethane (PUR) foams having immersed alumina powder. In the paper of Borsus a.o. [18] a fine and stable dispersion of alumina particles (having some –OH groups on the surface) in PUR foams was obtained through a molecular bridge between the particles and the organic polymer. During the curing process of the HTPB pre-polymer with the curing agent, the reaction between the alcohol (R-OH) and the isocyanate (R' –N=C=O) forms an urethane. The here used HTPB pre-polymer has a functionality equal to 2.2. Depending on the equivalent ratio R_{eq} between the curing agent and the binder, all the OH-groups of the per-polymer could be transformed in urethanes. Fig. 25 shows the curing process.
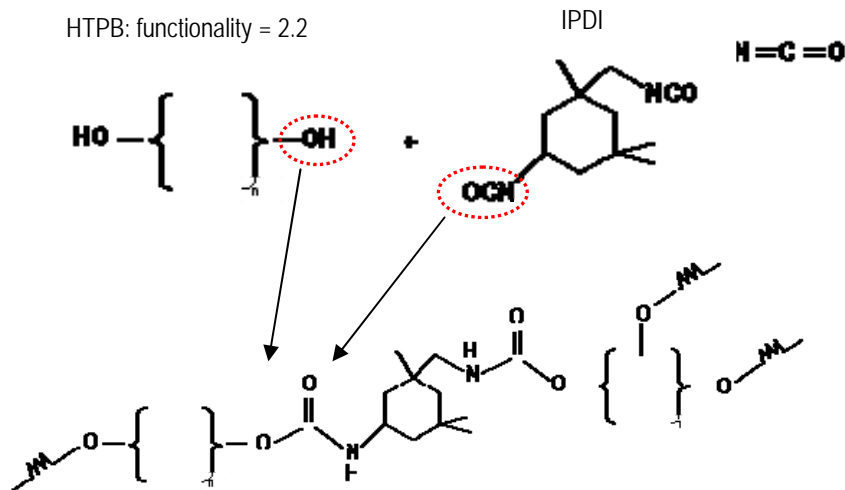

Figure 25: Scheme of the curing process of HTPB and IPDI.

It is known that nanoAl particles are covered by an oxide layer (Al_2O_3) that appears to be primarily amorphous [11]. A closer examination of the micrographs indicates that some areas of the oxide are arranged in sheets and contain a large fraction of hydroxide together with some other impurities. The outermost oxide layer is converted gradually to hydroxide if it is in contact with moisture. Several crystalline molecular layers can be seen to cover the oxide/hydroxide surface of the particles and the residual part of the oxide is amorphous with localised crystalline order in other areas [11,12]. For samples stored in humid environment the surface layer consists principally of aluminium hydroxide [11,13-16]. Results have shown that nanoAl absorbed more water compared to the micrometric Al, moreover the oxide/hydroxide surface of nanoAl has a highly porous structure.
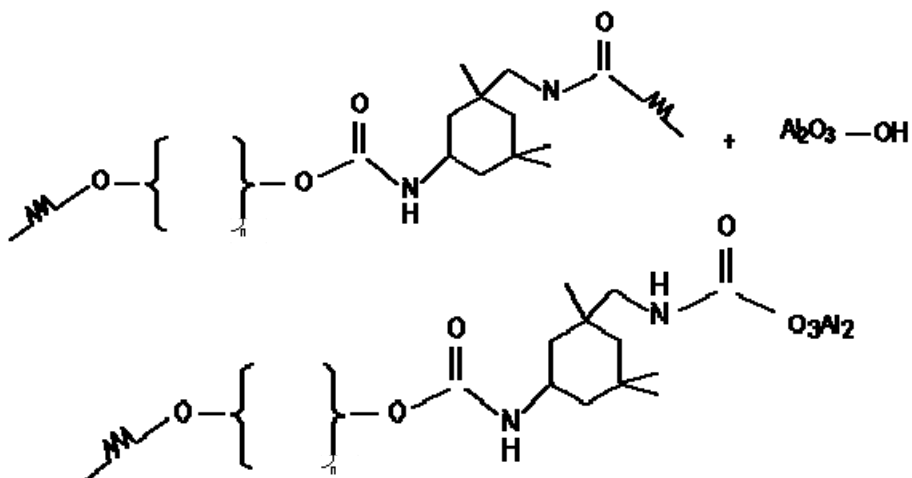

Figure 26: Scheme of the reaction between IPDI and the OH-groups on the surface of the nanoparticles.

The researchers mostly agree to consider this hydroxide as $Al(OH)_3$ [13-16] but for others it is $AlO(OH)$ [11,19]. Anyway, the crystalline layers appear to have some mismatch. Therefore exfoliation of the crystalline layers on the surface can explain the fast ageing characteristic of the nanoAl particles [19]. For the case discussed here the assumed presence of OH-groups on the particle surface interferes with the curing reaction and the following reaction scheme is proposed (Fig. 26). With ageing the active aluminium content (Al^0) of the nanoparticles decreases and the hydroxide content increases. The OH-groups are not homogeneously distributed on the surface and they can react with the curing agent (Fig. 26) giving a less cured propellant formulations.
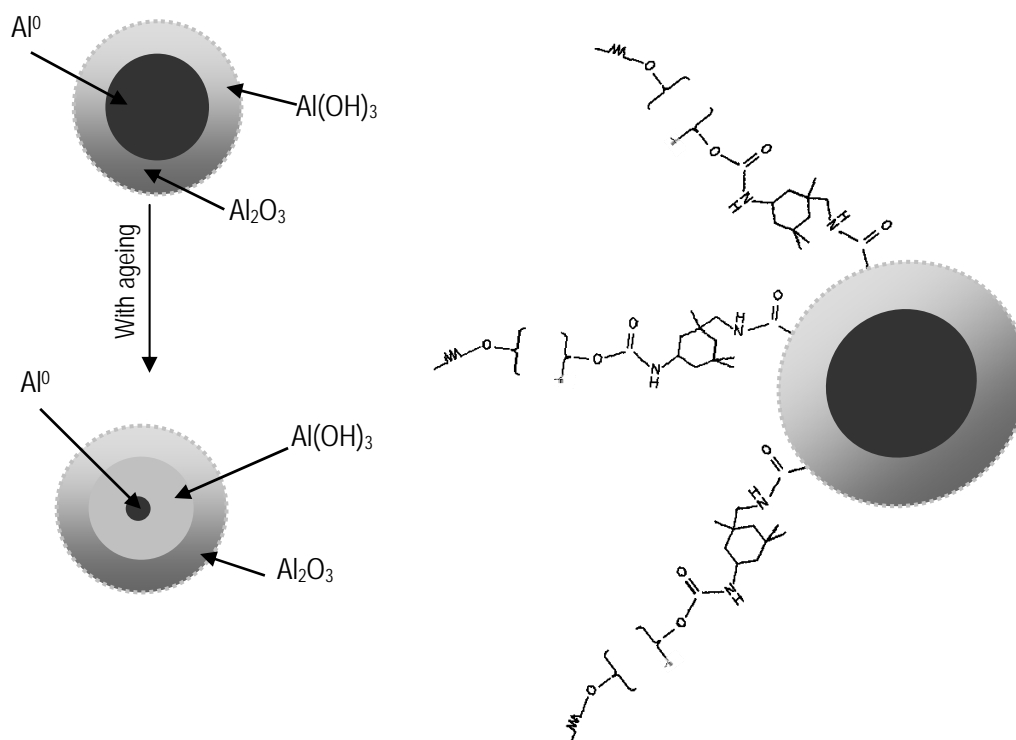

Figure 27: Scheme of the reaction of the Al nanoparticles with the curing agent.

By referring to the previous explanations, the soluble fraction of a formulation containing nanoAl should be higher than the one of propellants containing only microAl because the binder is assumed to be in an undercured condition by blocked IPDI and more free chains or only linked linear chains should be removable by the extraction solvent. However, the experimental results have evidenced lower values of the soluble part for the formulations containing nanoAl (Table 11). At the end of the Soxhlet extraction process of these formulations containing nanoAl (either in unaged or aged conditions) the glass filters have shown some black spots on the surface. If some chains (linear or cross-linked ones) are linked to the OH-groups present on the nanoAl surface, the solvent cannot remove them normally. But in the case it happens, due to the swelling phenomenon and thereby exerted forces, some nanoAl particles are pulled away from the specimen during the solvent take-up, and they are kept by the glass filter. Therefore, lower soluble fractions are measured as expected, when one assumes under-curing by blocking of IPDI by Al particles

4.3 GPC

The GPC analysis of the propellant extracts revealed clearly an extracted polymeric part. The molar mass distribution (MMD) of the polymeric part is located at substantially higher molar

masses as the pre-polymer HTPB R45M^{TM}. The low molar mass chains of HTPB are much less in occurrence probability in the extracts of the unaged propellant formulations than in HTPB. Most of the chains extracted are therefore longer than in HTPB. With ageing the MMD is shifted towards lower molar masses and narrows. The lower molar mass part increases relatively. This indicates chain scissioning. But because of the decrease in the extracted polymeric amount also bonding of these free chains to the polymeric network occurs. The GPC analysis provides also with quantitative information about the contents of Irganox 565 and DOA in the extract. The Irganox content decreases, which is interpreted as consumption by oxidative attack. The DOA content in the extracts increases with ageing, which is a pseudo increase because of real decrease in polymeric part. The mean molar masses Mn, Mw and Mz of the polymeric part decrease with ageing, whereby the Mz decreases with the highest rate. See Appendix 2 in [20] for the definition of these quantities This argues for the diminishing of the longer chains with a higher rate than for the shorter chains. Both mechanisms act in the same direction. The probability of chain splitting is larger for longer chains but also cross-linking to the binder network. With formulation AV03 an ageing series at three temperatures was analysed by GPC. From this Arrhenius parameters could be obtained for all quantities considered with GPC. The activation energies are similar to the ones found from SGA and from the modelling of the loss factor curves.

5 Conclusions

DMA (Dynamic Mechanical Analysis) in torsion mode and Sol-Gel-Analysis (SGA) were employed together with SEM and GPC (Gel Permeation Chromatography) to elucidate the ageing behaviour of four HTPB-based SRP formulations, whereby the particle size of aluminium powder and its content were changed. The accelerated ageing range was between 60°C and 90°C with ageing times adjusted to a thermal equivalent load of 15 to 20 years at 25°C. The results of all three methods (DMA, GPC and SGA) can be interpreted by the simultaneous presence of two competitive processes: chain scission and chain (re)combination with cross-linking. Arrhenius parameterisations were done with all measurement results. The activation energies obtained are similar in values meaning that with different analytical techniques the same phenomena were investigated and characterised.

The loss factor results were modelled with 3 exponentially modified Gauss (EMG) functions in order to get a molecular interpretation of the involved phenomena. The ageing of the propellant formulations can be followed regarding two parameters: the areas of the second and third transition peak named A_2, A_3 or the corresponding temperature values of the assigned Gauss peaks called Tc_2 and Tc_3. The modelling has also shown that the glass transition temperature of the phenomenological second peak ($T_g^{restricted}$) is composed of two different molecular phenomena represented by the transition temperatures Tc_2 and Tc_3. More detailed analyses can be achieved by investigation of model formulations designed in such a way to pronounce special effects and allow in this way a confirmation of the interpretations.

A statement has to be given to the use of nanoAl. The experimental results have underlined the importance of the use of coated nanoAl powders. The surface directly in contact with the binder must not be porous like Al_2O_3 in order to prevent or at least to reduce the diffusion of moisture in the bulk material. Moreover, also the presence of hydroxide must be eliminated because it has a strong effect on the NCO/OH ratio and on the course of the curing process of the propellant formulations.

6   Nomenclature

Symbols

A	Weighed-in amount of propellant for the extraction, [g]
Å	Ångström, unit of length, 10^{-10} m; 1 Å = 100 pm
A_i	Peak areas of the EMG peaks, also equivalent of area of the Gauss peaks alone, [°C]
A_k	Corrected amount of A ($A_k = A - A \cdot P_{Al} - A \cdot P_{AP}$), this is the weighed-in amount without filler parts, correction by nominal parts of Al and AP, [g]
A_{k-P}	Corrected amount of A, correction by the nominal parts of not considered components Al, AP, DOA, AO and if necessary other components, [g]
C	Cross-link density, [-]
E_a	Activation energy, [kJ·mol^{-1}]
EAn	Concentration normalized area of polymer eluate
E_{poly}	Polymeric part of total extract, corrected by nominal parts of plasticiser and AO, [g]
E_{total}	Total amount of extract gained by the method, [g]
G'	Storage modulus, [Pa]
G"	Loss modulus, [Pa]
I_{sp}	Gravimetric specific impulse, [s]
I_{spv}	Volumetric specific impulse, [N·s·dm^{-3}]
Mn	Polymer number per fraction averaged mean molar mass
Mw	Polymer mass per fraction averaged mean molar mass
Mz	Polymer z-weight per faction averaged mean molar mass
N	Number of fitting functions used in the EMG representation
NCO	Isocyanate group
OH	Hydroxyl group
P_{Al}	Nominal part of Al in composition, [-]
P_{AO}	Nominal part of AO in composition, [-]
P_{AP}	Nominal part of AP in composition, [-]
P_{DOA}	Nominal part of DOA in composition, [-]
RH	Relative Humidity
S_{prop}	Total soluble (extractable) part in the propellant sample, [-]
S_{poly}	Polymeric part of soluble part of composition with regard to A_{k-P}, [-]
S_{total}	Total soluble part with regard to A_k, [-]
T	Measurement temperature, [°C]
tan(δ)	Loss factor, tan(δ)=G'/G" [-]
tan(δ)$_{BLC}$	Value of the loss factor after the BLC as function of T, [-]
T_c	Flame temperature, [K]
Tc_i	Temperatures at peak maxima in the Gaussian part of EMG (not the peak maxima of EMG), [°C]
td_0	Offset in tan(δ) data (for these evaluations the value set to 0), [-]
t_E	Target time, [days]
T_E	Target temperature, [°C]
$T_g^{restricted}$	Glass transition temperature of the second peak of the loss factor, [°C]
$T_g^{unrestricted}$	Glass transition temperature of the first peak of the loss factor, [°C]
t_T	Test time at the test temperature T_T, [days]
T_T	Test temperature, [°C]
W_1	Mass of the dry glass extraction tube at start, [g]
W_2	Mass of the extraction tube + mass of the sample before the extraction (3.0±0.1 [g]), [g]
W_3	Mass of the extraction tube + mass of the sample after the extraction (after drying), [g]
w_i	Half peak width at half height of only Gaussian part, [°C]
δ	Phase angle in loss factor, [°]
τ_i	Relaxation parameter in exponential part of EMG, [°C]

Abbreviations

Al	Aluminium
AO	AntiOxidant
AP	Ammonium Perchlorate

BLC	BaseLine Correction
DLO	Diffusion Limited Oxidation
DMA	Dynamic Mechanical Analysis
DOA	DiOctyl Adipate, plasticiser
EDX	Energy Dispersive X-Ray
EMG	Exponentially Modified Gaussian
EOMV	End Of Mix Viscosity
erf	Error function
GPC	Gel Permeation Chromatography
HTPB	Hydroxyl-Terminated PolyButadiene
IPDI	IsoPhorone DiIsocyanate, curing agent
Irg	Irganox, antioxidant
MMD	Molar Mass Distribution
OB	Oxygen Balance
RI	Refractive Index
SEC	Size Exclusion Chromatography, synonymous to GPC
SEM	Scanning Electron Microscopy
SGA	Sol-Gel Analysis
SRM	Solid Rocket Motor
SRP	Solid Rocket Propellant
TEL	Thermal Equivalent Load
THF	TetraHydroFurane
TPB	TriPhenylBismuth, curing catalyst

Appendix: GPC measurement conditions

The GPC instrumentation is in detail a complex system. In the following the experimental information is given.

GPC column set used from company PSS (see below)

Polymer separation ranges in $g \cdot mol^{-1}$

PSS SDV 50 Å, 5µm	100 - 5 000
PSS SDV 100 Å, 5µm	100 - 10 000
PSS SDV 1000 Å, 5µm	100 - 60 000
PSS SDV 100 000 Å, 10µm	1000 - 1 000 000
PSS SDV pre-column, 5µm	

GPC columns of type analytical, single bed or single porosity (only one pore size per column)
separation material: porous divinyl benzene cross-linked polystyrene

average pore sizes in Å given with the column set

particle size: 5µm and 10µm, as indicated per column in the set compilation
column diameter: 8mm
column length: 30mm

Calibration was done with 19 narrowly distributed polystyrene standards in the range 162 to 246000 $g \cdot mol^{-1}$, obtained from company PSS. The calibration curve is shown in the Fig A1. The calibration was repeated at any change of the apparatus and before running a further sample set.

Column set temperature: 35°C
Measuring cell temperature of RI (refractive index) detector: 35°C
eluent or mobile phase: THF (tetrahydrofuran)
eluent flow rate: 1 $ml \cdot min^{-1}$
sample solution solvent: THF
sample solution injection volume: 100µl
typical sample concentration in THF: 2.5 to 3.5 $mg \cdot ml^{-1}$

Instrumentation

isocratic high pressure pump, autosampler and RI-detector from company Agilent, type 1100 Series
column oven type T-1000 from company WEG Dr. Bures, Berlin, Germany
solvent degasser from company Uniflows Co., Tokyo, Japan, type Degasys Populaire DP 4003

GPC software from company PSS; Software-Version: PSS WinGPC Unity Build 6807
PSS Polymer Standards Service GmbH
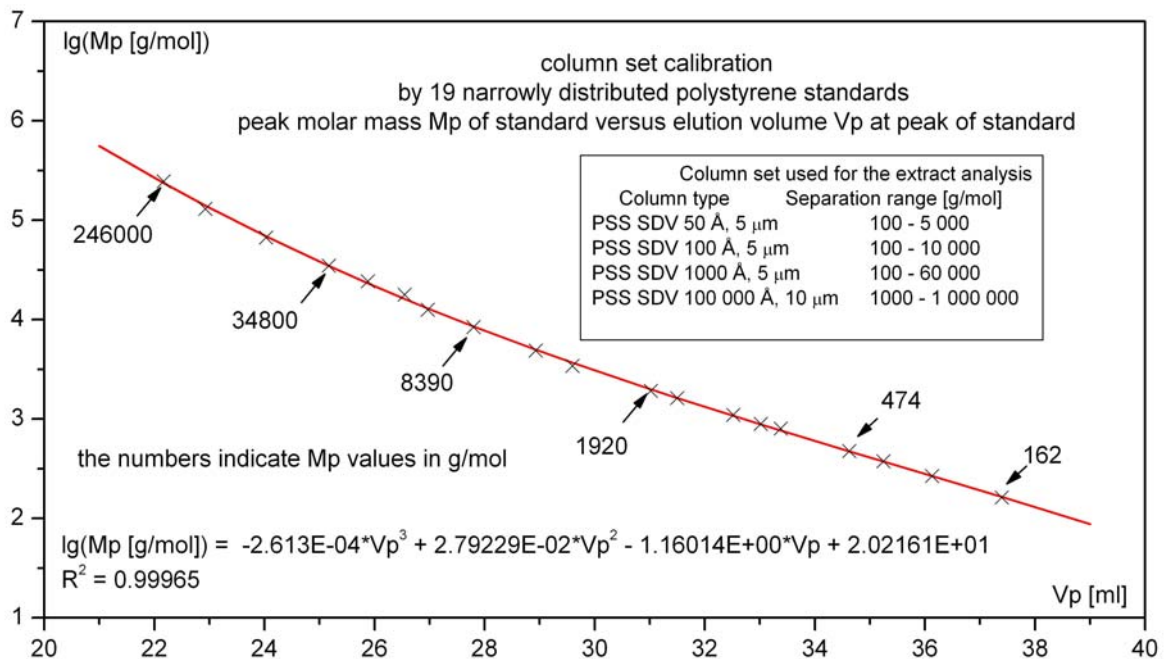PO-BOX 3368
D-55023 Mainz
Germany

Figure A1: Calibration curve of the used GPC column set

References

[1]   Shalom A., Aped H., Kivity M., Horowitz D.
The Effect of Nanosized Aluminum on Composite Propellant Properties, in proc. *41st AIAA/ASME/SAE/ASEE Joint Propulsion Conference and Exhibit*, Tucson, Arizona, AIAA Paper 2005-3604, 10-13 July **2005**.

[2]   Bui D.T., Atwood A.I., AtienzaMoore T.M.
Effect of Aluminum Particle Size on Combustion Behavior of Aluminized Propellants in PCP Binder, in proc. *35th International Annual Conference of ICT*, Karlsruhe, Federal Republic of Germany, 29 June-2 July, **2004**.

[3]   Lessard P., Beaupré F., Brousseau P.
Burn rate studies of composite propellants containing ultra-fine metals, in proc. *32nd International Annual Conference of ICT*, Karlsruhe, Germany, 3-6 July, **2001.**

[4]   Bohn M.A.
Prediction of equivalent time-temperature loads for accelerated ageing to simulate preset in-storage ageing and time-temperature profile loads, in proc. *40th International Annual Conference of ICT*, Karlsruhe, Germany, 23-26 June, **2009**.

[5]   Cerri S., Bohn M.A., Menke K., Galfetti L.
Ageing Behaviour of HTPB Based Rocket Propellant Formulations, *Central European Journal of Energetic Materials*, Vol. 6, No. 2, p. 149-165, **2009**.

[6]   Cerri S., Bohn M.A., Menke K., Galfetti L.
Ageing Behaviour of Composite Racket Propellant Formulations, *3rd European Conference for Aerospace Science (EUCASS)*, Versailles, France, 6-9 July, **2009**.

[7]   Charlesby A.
Atomic Radiation and Polymers, Pergamon Press, Oxford, p. 68, 1960

[8]   STANAG 4581, *Explosives, Assessment of Ageing Characteristics of Composite Propellants Containing an Inert Binder*, Military Agency for Standardization, NATO, Final Draft Edition, October, **2003**.

[9]   Kumar A., Commereuc S., Verney V.
Ageing of elastomers: a molecular approach based on rheological characterization, *Polymer Degradation and Stability*, Vol. 85, p. 751-757, **2006**.

[10] Lepie A., Adicoff A.
Dynamical Mechanical Behavior of Highly Filled Polymers: Dewetting Effect, *Journal of Applied Polymer Science*, Vol. 16, p. 1155-1166, **1972**.

[11] Ramaswamy A.L., Kaste P.
A 'Micro-vision' of the Physio-chemical Phenomena Occuring in Nanoparticles of Aluminum, *Journal of Energetic Materials*, Vol. 22, No. 1, p. 1-24, **2004**

[12] Gerstman V.Y., Kwok Q.S.M.
TEM Investigation of Nanophase Aluminum Powder, *Microscopy and Micronalysis*, Vol. 11, p. 410-420, **2005**.

[13] Cliff M., Tepper F., Lisetsky V.
Ageing Characteristics of Alex® Nanosize Aluminum, in proc. *37th AIAA/ASME/SAE/ASEE Joint Propulsion Conference and Exhibit*, Salt Lake City, Utah, AIAA Paper 2001-3287, 8-11 July, **2001**.

[14] Brousseau P., Crête J.-P., Dubois C.
Ageing of Polymer-Coated Ultra-Fine Particles, in proc. *36th International Annual Conference of ICT together with the 32nd International Pyrotechnics Seminar*, Karlsruhe, Germany, 28 June-1 July, **2005**.

[15] Meda L., Marra G., Galfetti L., Severini F., DeLuca L.
Nano-aluminum as energetic material for rocket propellants, *Material Science and Engineering C*, Vol. 27, p. 1393-1396, **2007**.

[16] Galfetti L., DeLuca L.T., Severini F., Meda L., Marra G., Marchetti M., Regi M., Bellucci S.
Nanoparticles for solid rocket propulsion, *Journal of Physics: Condensed Matter*, Vol. 18, p. S1991–S2005, **2006**.

[17] Doi Masao, Edwards S.F., The Theory of Polymer Dynamics, Clarendon, Oxford, **1986, 2001**.

[18] Borsus J.M., Merckaert P., Jérôme R., Teyssié P.H.
Enhancement ofAdhesion between Filler and Polymer in Alumina-Filled Rigid Polyurethane Foams", *Journal of Applied Polymer Science*, Vol. 29, pp. 1857-1863, **1984**.

[19] Ramaswamy A.L., Kaste P.
A 'Nanovision' of the Physiochemical Phenomena Occuring in Nanoparticles of Aluminium, *Journal of Energetic Materials*, Vol. 23, No. 1, p. 1-25, **2005**.

[20] Cerri S., Bohn M.A., Menke K., Galfetti L.
Ageing of HTPB/Al/AP rocket propellant formulations investigated by DMA measurements, Sol-Gel and GPC Analysis.
Paper 42, pages 42-1 to 42-38 in Proceed. of 41th International Annual Conference of ICT on 'Energetic Materials – High Performance, Insensitive Munitions, Zero Pollution', June 29 to July 2, 2010, Karlsruhe, Germany. ISSN 0722-4087. Fraunhofer-Institut für Chemische Technologie (ICT), D-76318 Pfinztal-Berghausen. Germany, **2010**.

[21] Cerri S., Bohn M.A.
Separation of molecular mobility ranges in loss factor curves by modelling with exponentially modified Gauss distributions.
Paper 87, pages 87-1 to 87-16 in Proceed. of 41th International Annual Conference of ICT on 'Energetic Materials – High Performance, Insensitive Munitions, Zero Pollution', June 29 to July 2, 2010, Karlsruhe, Germany. ISSN 0722-4087. Fraunhofer-Institut für Chemische Technologie (ICT), D-76318 Pfinztal-Berghausen, Germany, **2010**.